

## A. Point by Point Response to Reviews

Dear anonymous reviewers,

Thank you for your thorough reviews and your support in improve this manuscript.

### Response to Reviewer 1

**Line 31. Are you sure that “the summer drawdown for COS is 6 times stronger than for CO<sub>2</sub>”? The magnitude of the times seems too large to be believable.**

*The exact wording of the cited paper Montzka et al. (2007) is:*

*‘However, while reduced mixing ratios of CO<sub>2</sub> during the NH growing season represent a balance between vegetative uptake and total respiration (i.e. NEP), the percentage reduction on COS mixing ratio is 4-6 times (5.5+/- 1.6) larger during June- August (calculated relative to mixing ratios measured at 4-8 km asl) (Figure 6c).’*

*We reworded the sentence to more accurately correspond to the cited paper (Montzka 2007):*

However, the relative decrease in ambient mixing ratio during summer of the northern hemisphere is 6 times stronger for COS than for CO<sub>2</sub> (Montzka et al., 2007) as COS is generally not emitted by plants like CO<sub>2</sub>, which is released in respiration processes.

**Line 130. “while air was sucked through the chamber to the QCL at a flow rate of 1.5 l min<sup>-1</sup>”. The heights of air inlets for the chamber and ambient environment should be noted because remarkable vertical distribution of COS mixing ratio near the ground was observed in this study. If the height of air inlet for the chamber was within the canopy of the grass, the COS uptake flux would be largely overestimated, e.g., the COS mixing ratio could drop to 134ppt within the canopy in comparison with about 500ppt over the canopy.**

*The intake height was at 0.12 m above the ground and thus within the canopy. The COS concentration inside the chamber was thus similar to what the undisturbed soil would experience, which avoids uptake/release being biased high/low when COS-enriched air from above the canopy would be used.*

*We included this information in the method section.*

*The intake height of the ambient as well as the inlet of the chamber air were located at 0.12 m above the ground and thus within the canopy height with the exception of right after the cuts (see cutting dates in Section 2.1).*

*However, we also have to disagree with the comment on the overestimation of the uptake flux if the intake was within the canopy. In order not to bias measurements, the mixing ratios used for chamber flux measurements should be as close to reality as possible, which is why air from within the canopy was used. Had we used COS-enriched air from above the canopy, any soil uptake would have been overestimated (because the COS gradient across the soil surface is increased), while any COS emission would have been underestimated (because the COS gradient across the soil surface is reduced).*

*We added this information to the discussion:*

The low COS mixing ratios observed in the lowermost canopy layers just above the soil surface emphasize the importance of using air from within the canopy for soil chamber measurements and not COS richer air from above the canopy, which would increase the COS gradient and thus increase uptake/decrease emission of COS to/from the soil.

**Line 228. What’s the plant available water? Fig. 1 only presents the SWC (%) which is below 38% during almost all days, rather than 21 days.**

*The SWC in Fig.1 was replaced with the plant available water, which falls below 50 % during 111 days.*

**Line 248. “During nighttime (RSW = 0, n = 43), the soils of the grassland acted as a net sink for COS 74.4 % of the time” is better replaced by “During nighttime (RSW = 0, n = 43), 74.4 % of the COS emission fluxes were negative, implying soils of the grassland acted as a net sink for COS”.**

43 *The sentence was changed as suggested.*

44 **Line 263. Why did you use both circles and open diamonds for depicting COS soil fluxes? What's the difference**  
45 **between them?**

46 *We removed the depiction about the open diamonds, which were not present in the plots.*

47 **Lines 276-278. “Especially after the cuts we observed a strong decline in COS uptake and even times where the**  
48 **grassland turned into a net source for COS with midday means of up to 24.5 pmol m<sup>-2</sup>s<sup>-1</sup> (Fig. 4 b) for up to 8 days**  
49 **after the cut, when the dried litter had already been removed (Fig. 2 a-c)”.** This sentence is suggested to be replaced  
50 by “Especially after the cuts we observed a strong decline in COS uptake ((Fig. 4 b)) and the grassland even turned  
51 into a net source for COS in middays (Fig. 2 a-c) with a highest emission flux of 24.5 pmol m<sup>-2</sup>s<sup>-1</sup> in August after the  
52 cut.”.

53 *We replaced the sentence according to your suggestion. To keep the crucial information about the grassland turning into a*  
54 *net source for up to 8 days after the cut, we added an additional sentence to the manuscript:*

55 *We observed COS emissions for up to 8 days after the cut, when the dried litter had already been removed (Fig. 2 a-c).*

56 **Lines 280-281. “The cut in October led to a reduction in COS uptake, which was lowest three days after the cut (Fig.**  
57 **2d)”.** The description seems to be inconsistent with the Fig. 2d.

58 *We agree that the lowest COS uptake did occur later than 3 days after the cut. However, this is also related to the overall*  
59 *decline in COS uptake by the grassland at the end of the season. We see no recovery of the COS flux after the last cut. We*  
60 *rephrased this in the manuscript and included more data points to Fig. 2 d):*

61 *The cut in October led to a reduction in COS uptake, which declined across several days and did not recover, as the end of*  
62 *the season was reached (Fig. 2 d & Fig. 5 b).*

63 **Lines 297-298. I don't understand the meaning of the sentence. Fig. 4a is the seasonal cycle of CO<sub>2</sub>, rather than COS.**

64 *We changed Fig 4a to 4c and added Fig 4a to subsequent sentence dealing with the seasonal response of respiration.*

65 **Lines 325-328. I wonder why the COS mixing ratio dropped so large during the nighttime when the COS uptake was**  
66 **much less than that during midday.**

67 *Compared to the constant influx of COS rich air during daytime, due to the increased boundary layer (see line 422), this*  
68 *influx stops during nighttime and COS gets depleted within the canopy, even when the COS uptake of the ecosystem is lower*  
69 *than during daytime. The strong input of COS rich air during daytime has also been reported by other studies.*

70 *We added references to the manuscript (Campbell 2017 & Rastogi 2018).*

71 **Lines 375- 377. I don't understand the logic of this sentence. Because the chamber enclosed both soil and the residual**  
72 **grass after the cuts, the COS emission under sunlight irradiation might be due to the residual rather than the soil**  
73 **itself, e.g., the photochemical formation of COS from the possible liquid released from the cut grasses (JGR, 109,**  
74 **D13301, doi:10.1029/2003JD004206, 2004; JES, 5 1 ( 2 0 1 7 ) 1 4 6 – 1 5 6).** If the COS emission was ascribed to soil,  
75 **the authors are suggested to verify it by using a flow tube method under dark and irradiation conditions.**

76 *We removed this sentence.*

77 **Line 413. Why did the lowest COS mixing ratio appear in winter when vegetation COS uptake is relatively low?**

78 *During winter, no strong emission fluxes are expected to originate from vegetation and soils. The mixing ratios rather*  
79 *depend on the transport of COS enriched air from oceans, which are also highest in summer (see Montzka 2007).*

80

81 **Lines 419-421: The above sentences didn't mention the difference in concentrations during day and nighttime.**

82 *We added the sentence:*

83 *Even though the COS mixing ratio at the layer closest to the soil were higher during day than during nighttime, the absolute*  
84 *decrease in COS was lower during nighttime due to partial stomatal closure (Kooijmans et al., 2017; Campbell et al., 2017).*

85 *The absolute difference in concentrations during day and nighttime originate from changes in the height of the planetary*  
86 *boundary layer (PBL).*

87

88 **Lines 421-422. Considering the much stronger COS uptake by the grass in daytime than in nighttime, COS mixing**  
89 **ratio above the canopy should decrease in daytime, rather than nighttime despite of the variation of PBL**

90 *Several studies (e.g. Rastogi 2018 – Ecosystem fluxes of carbonyl sulfide in an old-growth forest: temporal dynamics and*  
91 *responses to diffuse radiation and heat waves) showed that the PBL is the main influence factor on sub-diurnal variability in*  
92 *COS mixing ratio. The incomplete stomatal closure as well as the soil sink cause the nighttime decrease in mixing ratio as*  
93 *there is no influx of COS rich air from the atmosphere. The stronger daytime drawdown can also be observed in the gradient*  
94 *analysis as the decrease in COS mixing ratio, from to the canopy height down to the soil was higher during daytime (125*  
95 *ppt) compared to the nighttime decrease (102 ppt).*

96 *This information is already present in the manuscript; see line 325-328 and 419-423.*

97

98 **Response to Reviewer 2**

99 **1. Definition of “LRU on ecosystem scale”: note that most LRUs in the literature were derived from branch chamber**  
100 **measurements, and were then used in the relationship between Fcos and Fco2 (Eq.1), with the implication/assumption**  
101 **that LRUs derived from branch chamber measurements are representative of the entire canopy. Here the authors**  
102 **infer the LRU (of the entire canopy) from ecosystem flux measurements. Please clarify this.**

103 *We added that the LRU was calculated using eddy fluxes without the need to use chambers to the method section:*

104 *Using the above stated method infers LRU solely on the basis of fluxes on ecosystem scale, whereas other studies typically*  
105 *used branch/leaf chamber measurements (Yang et al., 2018) to determine the relationship between the COS and CO2 uptake*  
106 *rates.*

107 **2. CO2 observations: IRGA CO2 measurements were used in the analyses. I believe that the QCL also measured**  
108 **CO2. Were those data used somehow? If IRGA CO2 measurements were calibrated to the WMO scale, CO2 should**  
109 **be reported as mole fractions instead of mixing ratios, because the WMO scale (NOAA calibration gases) is reported**  
110 **on mole fractions. The difference between mole fractions and mixing ratios is significant for CO2, and not significant**  
111 **for COS.**

112 *The COS and CO2 fluxes were calculated using solely the QCL data as stated in section 2.5.2. We followed the processing*  
113 *steps of Gerdel et al. 2017 to retrieve the fluxes using the same filters, which as stated by Gerdel et al. 2017 has the*  
114 *advantage that the influence of the high pass filter on the ecosystem relative uptake (ERU) largely cancels out, if applied on*  
115 *COS as well as CO2. The ambient COS and CO2 concentrations both originated from the QCL data, which puts out mixing*  
116 *ratios. We changed the method section accordingly since neither CO2 nor H2O fluxes of the IRGA were used in the final*  
117 *version of the manuscript. We apologize for the confusion.*

118 **3. What are the reasons for the relatively low enhancements of daily maximum PAR values reaching the soil surface**  
119 **after the third and the fourth cuts (Figure 1)? These are not consistent with the “incident shortwave radiation**  
120 **reaching the soil surface” in Figure 3e.**

121 *The data of the PAR reaching the soil surface in Fig 1 originated from a PAR sensor that was likely overgrown by short*  
122 *vascular plants and mosses growing directly at the soil surface at the end of the season. We changed the data from this*  
123 *sensor to the data of Fig 3e, which was calculated using the Beer-Lambert law (see line 151).*

124 **4. Fcosmedian turned to positive after the third cutting while remained largely negative after the fourth cutting**  
125 **(Figure 2c&d), given that COS soil fluxes would be both positive. What could explain the difference here?**

126 *The modelled soil fluxes were always relatively small compared to the ecosystem scale fluxes and shouldn't be the reason for*  
127 *the difference between fig 2c&d. Also, there is less incoming solar energy at the end of the season, likely also decreasing the*  
128 *emission strength of the residual litter.*

129 *We added a sentence containing this to the discussion:*

130 *We did not observe strong COS emissions after the last cut, as the incoming solar radiation, which we hypothesize to amplify*  
131 *the degradation of sulfur containing compounds of plants, was reduced at the end of the season.*

132 **5. High-light conditions: what is the definition of high-light conditions? How sensitive is the estimated LRU at high**  
133 **light intensity to the choice of high-light conditions?**

134 *The parameter "iota" – LRU under high light conditions results from equation 8. The second parameter "kappa" controls*  
135 *the exponential decrease of LRU when the incoming photosynthetic active radiation (PAR) is decreasing and limiting GPP*  
136 *but not the COS flux.*

$$LRU = \iota e^{\left(\frac{\kappa}{R_{PAR}}\right)}$$

137 *While mathematically iota is only obtained at infinitely high PAR, in practice above about 700  $\mu\text{mol m}^{-2} \text{s}^{-1}$  PAR only*  
138 *insignificant change in the ecosystem relative uptake, reflecting the relationship between the COS and the  $\text{CO}_2$  flux, can be*  
139 *observed.*

140 *We included the definition for high light into the methods part:*

141 *While mathematically  $\iota$  is only obtained at infinitely high PAR, in practice above about 700  $\mu\text{mol m}^{-2} \text{s}^{-1}$  PAR (Kooijmans et*  
142 *al., 2019) only insignificant change is reported in other studies (Stimler et al., 2011).*

143 **Other technical comments:**

144 **Line 111: I think it is more likely by a GC-MS than a GC, please double check.**

145 *We changed GC to GC-MS within the revised document.*

146 **L154: The unit of RSW-soil should be  $\text{Wm}^{-2}$ , and for other places as well.**

147 *We changed this according to the reviewer comment.*

148 **L165: obtain-high resolution ! obtain high-resolution**

149 *We changed this according to the reviewer comment.*

150 **L191: Eq.7 was developed in earlier studies, please refer to the original work.**

151 *We changed this according to the reviewer comment and added (Sandoval-Soto 2005) as reference.*

152 **L198-203: It will read better if these are moved to after L188.**

153 *We changed this according to the reviewer comment.*

154 **L230: It needs a bit more explanation of NDVI, what does it indicate?**

155 *We changed the manuscript accordingly.*

156 **Figure 3 caption. open diamonds?**

157 *We removed the text part about the open diamonds, which are not present in the figure.*

158 **L312: why is an increase in RECO expected?**

159 *Even though there is a reduction in plant respiration, the increase in incoming radiation reaching the soil surface leads to*  
160 *an increase in soil temperature and consequently soil respiration (see Fig.5a). We added this information to the manuscript:*

161 *While the grassland acted as a net sink for  $\text{CO}_2$  during periods of high LAI (Fig. 5 6 b), a combination of a decline in GPP*  
162 *and an increase in daytime RECO, as more incoming radiation was heating the soil surface, turned it into a net source*  
163 *during midday in periods of low LAI (Fig. 5 6 a).*

164 **L319: should be COS instead of  $\text{CO}_2$**

165 *We changed this according to the reviewer comment.*

166 **L433-435: LRU is a normalized ratio, and should not depend on the ambient COS. I do not get the point here.**  
167 *This is not quite right. LRU is calculated in order to normalize for differences in COS (and CO<sub>2</sub>) concentrations, which*  
168 *affect the fluxes. For the same COS and CO<sub>2</sub> flux and the same CO<sub>2</sub> concentration, LRU will differ whether the ambient*  
169 *COS concentration is 400 or 500 ppt. This is what we quantified in the linear perturbation analysis and what this sentence*  
170 *refers to.*

171 **L437-439: Please specify which are the exact “those observations”. Figure 4 indicates that low COS fluxes took place**  
172 **shortly after the cuttings, which coincides with COS emissions from soils after the cuttings.**

173 *We clarified this by changing the sentence to:*

174 *For the calculation of LRUs we had to remove the canopy flux data containing COS and/or CO<sub>2</sub> emissions observations*  
175 *since these would yield negative values for ERU and LRU (see Eq.8).*

176 **L419-422: It may be worth pointing out that the vertical gradient of COS between the canopy level and below the**  
177 **canopy levels exists throughout the day and night, but that of CO<sub>2</sub> does not.**

178 *We added the information to the discussion.*

179 *We only observed an increase in CO<sub>2</sub> mixing ratios, caused by the release of CO<sub>2</sub> through respiration processes in the soil,*  
180 *whereas COS mixing ratios further declined down to the soil surface.*

181

## 182 Response to Reviewer 3

183 **Minor comments in general:**

184 **There seems to be a really strong gradient within the grass canopy. Would the really low COS above the soils (100-**  
185 **200 ppt) influence the COS flux?**

186 *Yes, since the exchange across the soil surface is driven by the concentration gradient between the ambient air just above*  
187 *the soil surface and within the soil. We added a sentence containing this information to the discussion:*

188 *The low COS mixing ratios observed in the lowermost canopy layers just above the soil surface emphasize the importance of*  
189 *using air from within the canopy for soil chamber measurements and not COS richer air from above the canopy, which*  
190 *would increase the COS gradient and thus increase uptake/decrease emission of COS to/from the soil.*

191 **Out of interest, what does the FCOS/[COS] (COS deposition velocity) look like?**

192 *We provide the plot in the revised supplement.*

193 **I also think the concentration discussion (Sections 3.4, Fig 6, 4.3) should come before the flux discussion. It really sets**  
194 **the context to fully appreciate the flux discussion.**

195 *We agree and moved the parts accordingly.*

196 **Data needs to be made public before publication! Make sure in the final version that the text in the figures is big**  
197 **enough. I was having to zoom in a lot to read things.**

198 *The data is online now and the font size of the text within the figures was increased.*

199 **I'm really impressed at how well the FP+ model works for grass (Fig 5b/d).**

200 *Thank you, we were also very happy with the mean diel fluxes resulting from the model.*

201 **What drives the large change in CO<sub>2</sub> variability between day and night?**

202 *As shown by Wohlfahrt et al. (2005), the large variability of NEE during nighttime conditions is due to the combination of*  
203 *low wind speeds and stable stratification which results in highly intermittent CO<sub>2</sub> fluxes compared to well-mixed convective*  
204 *daytime conditions. On a half-hourly basis, fluxes may even be negative (i.e. net uptake of CO<sub>2</sub>), which is biologically*  
205 *impossible, but results from the intermittent nature of the CO<sub>2</sub> transport and is typically compensated for by large emission*  
206 *fluxes in a subsequent averaging period. As recommended by Wohlfahrt et al. (2005), CO<sub>2</sub> fluxes were filtered for u\*, but not*  
207 *for the sign of the fluxes in order not to bias nighttime fluxes towards too large CO<sub>2</sub> emission.*

208 *We added this reference and information to the manuscript.*

209 **#Has the data been filtered for  $u^*$ ? Has any of this large variability been taken into account in the Reco vs temp**  
210 **calculation for GPP uncertainty (something to think about in future if not?).**

211 *The data has unintentionally not been filtered for  $u^*$ . We determined the threshold at  $\sim 0.2 \text{ m s}^{-1}$  for  $\text{CO}_2$  and used the same*  
212 *value for COS. After reanalyzing the data, we observed only minor changes and no changes in the overall patterns. Text and*  
213 *figures were adapted accordingly. We attached all plots before and after the correction at the end of this document. During*  
214 *the reanalysis we were also able to recover more data from immediately after the first cut, which slightly increased LRU and*  
215 *ERU during this phase in Fig. 7a.*

216 **There is a little repetition with the Results and Discussion being separate. I wouldn't object if the authors decided to**  
217 **combine both and tightened the text up. But obviously that's just a suggestion.**

218 *We thank reviewer 3 for the advice but prefer to keep the sections separated.*

219 *We removed several redundancies.*

220 **Minor comments by line number:**

221 **14: soil flux**

222 *We changed this according to the reviewer comment.*

223 **31: do you mean relative uptake? COS is in ppt vs  $\text{CO}_2$  in ppm**

224 *Yes, we reworded the sentence to more accurately correspond to the cited paper (Montzka 2007):*

225 *However, the relative decrease in ambient mixing ratio during summer of the northern hemisphere is 6 times stronger for*  
226 *COS than for  $\text{CO}_2$ , (Montzka et al., 2007) as COS is generally not emitted by plants like  $\text{CO}_2$ , which is released in*  
227 *respiration processes.*

228 **38: Extra bracket**

229 *We added a comma and removed the bracket.*

230 **86: What kind of fertilizer (dairy? beef? pig?)? And when was it fertilized previously? Before the winter?**

231 *The grassland is fertilized with solid manure and cattle slurry (see Hörtnagl et al. 2018) once a year at the end of the*  
232 *growing season in October. We added the information to the manuscript:*

233 *Each year, the field site was fertilized with solid manure and cattle slurry (Hörtnagl et al., 2018) at the end of the season*  
234 *(07.10. in 2015).*

235 **140: Ambient COS from what height? There is a massive COS gradient so this will be important.**

236 *The intake height was at 0.12m above the ground and thus within the canopy with the exception of measurements taken just*  
237 *after the cuts. This information is now included in the method section:*

238 *The intake height of the ambient as well as the inlet of the chamber air were located at 0.12 m above the ground and thus*  
239 *within the canopy height with the exception of measurements right after the cuts (see cutting dates in Section 2.1).*

240 **160: I think this needs more explanation. What does an OBB represent? Is that good? Not good? If you aren't going**  
241 **into enough detail for readers to evaluate the model, then cut it. It's kind of hanging there with not enough info. And**  
242 **most of the packages mentioned will represent some mathematical approach to data analysis. Since packages come**  
243 **and go, it would be really helpful to have a sentence or two about what these packages actually represent.**

244 *The OOB score can be interpreted as a pseudo- $R^2$  and is widely used in random forest analyses (regression and*  
245 *classification), especially in the absence of a proper test dataset. It uses the data not seen by the trees (random forest uses*  
246 *bootstrapping) as a test dataset. We added this information to the methods section.*

247 **168: What heights along the tower were the gradients sampled from? How often were they sampled vs eddy flux**  
248 **sampling?**

249 *The information was already present in the methods section. See 2.3 and 2.3.1*

250 **173: Was the eddy flux data filtered for insufficient turbulence? If so, what  $u^*$  filter was applied? How was the  $u^*$**   
251 **threshold quantified? A plot of the FCOS and FCO<sub>2</sub> vs  $u^*$  would be helpful here to understand the micro met**  
252 **dynamics for the site.**

253 *The  $u^*$  threshold was determined by running the change point detection algorithm of Barr et al (2013) on nighttime NEE.*

254 *The  $u^*$  for the CO<sub>2</sub> flux ( $\sim 0.2 \text{ m s}^{-1}$ ) was then applied for COS. We also tried to determine the  $u^*$  threshold for COS, but a*  
255 *satisfying change point couldn't be determined.*

256 *We noticed that the eddy flux data was unintentionally not correctly filtered for  $u^*$  in the plots (which almost exclusively has*  
257 *only an effect during the night). The data in the plots and the corresponding values in the text have been updated.*

258 *We added the plot of the FCO<sub>2</sub> vs  $u^*$  to the supplement.*

259 **329: What does the [CO<sub>2</sub>] drop down to? Is there a relationship between  $u^*$ /turbulence and the d[COS] and d[CO<sub>2</sub>]?**  
260 **That would be an interesting figure to see.**

261 *The CO<sub>2</sub> mixing ratio drops down to 339 ppm at 0.1m above ground at 10 a.m. We added a plot containing the  $u^*$  values*  
262 *and the differences of the CO<sub>2</sub> and COS mixing ratios between canopy level (0.4m) and 0.02 m for COS and 0,1m for CO<sub>2</sub> to*  
263 *the supplement. The two lowest measurement heights were excluded for CO<sub>2</sub> since there the CO<sub>2</sub> mixing ratio increased due*  
264 *to the soil respiration.*

265 **422: How long does the morning increase in COS last for? Do you start to see a decrease in COS as the daytime**  
266 **uptake influences the air in the valley? Other sites have also seen this morning peak in COS. Maybe include a**  
267 **reference to those here. (e.g. Redwoods, Harvard Forest, etc)**

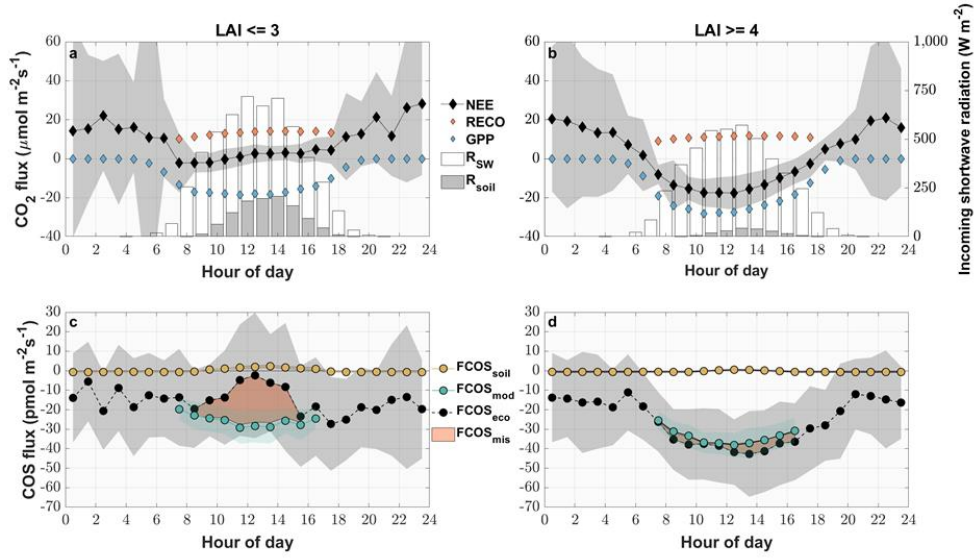
268 *We observed a steep morning increase in COS mixing ratios until about 11 a.m.. We included include this plot in the*  
269 *supplement and added the requested information to the discussion.*

270 *While the PBL is shallow during nighttime and the COS mixing ratio decreases due to the sink strength of the grassland, at*  
271 *the onset of the day, the PBL layer height increases quickly and COS rich air is transported down to the ecosystem (see Fig.*  
272 *S12) (Campbell et al., 2017). A similar steep increase until midday has also been observed by Rastogi et al. (2018).*

273

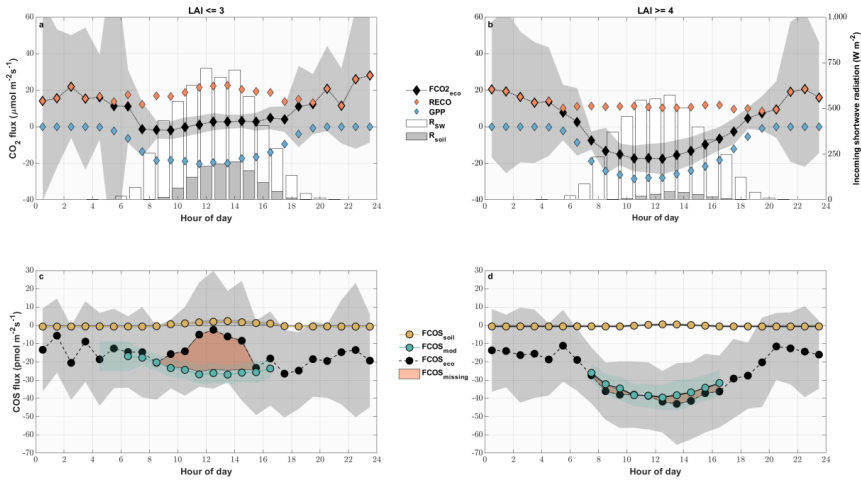
274 Updated figures:

275 New:



276

277 Old:

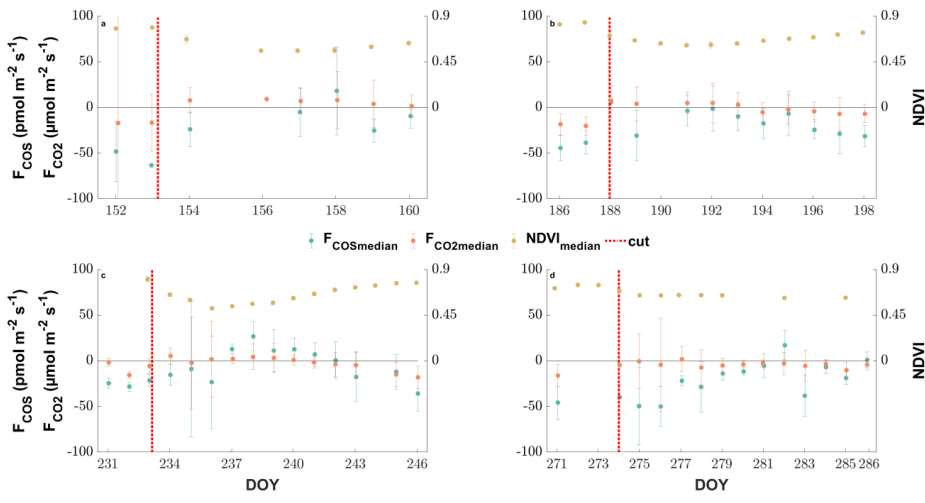


278

279

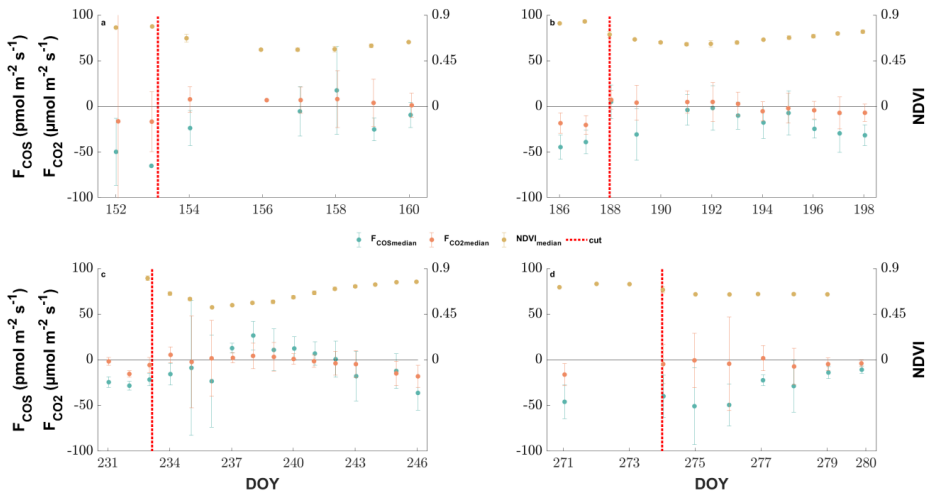


280 *New:*



281

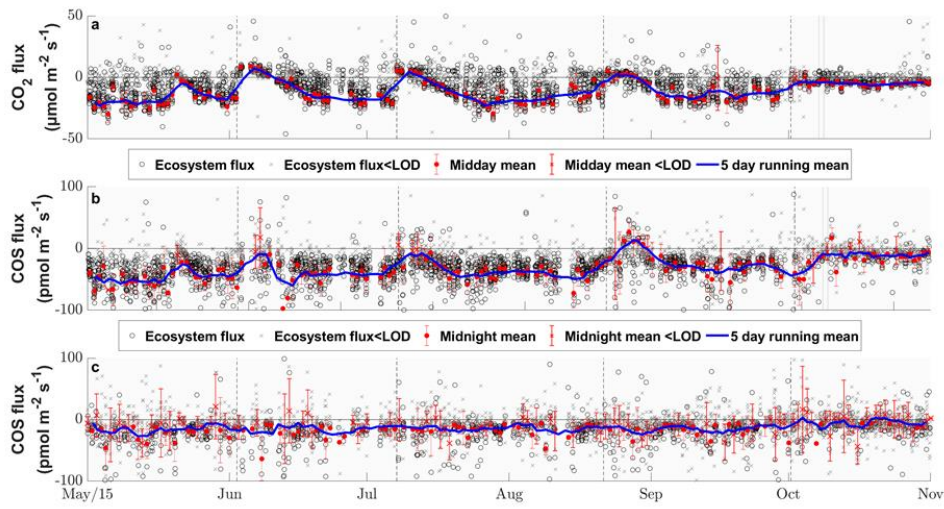
282 *Old:*



283

284

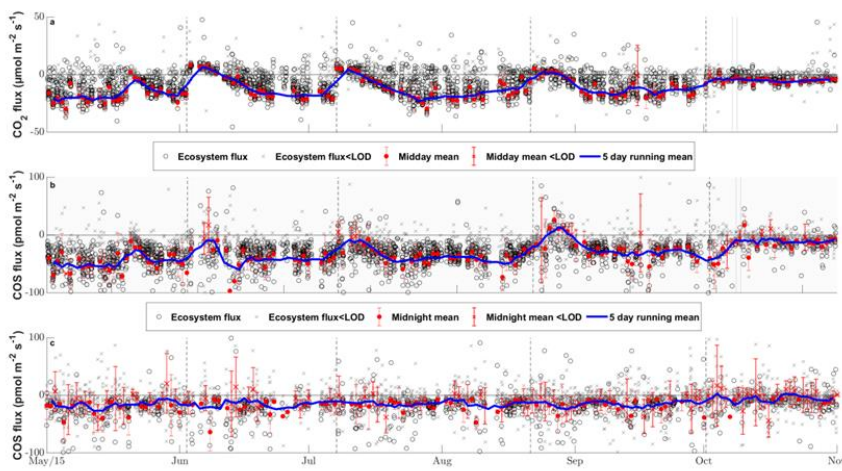
285 *New:*



286

287 *Old:*

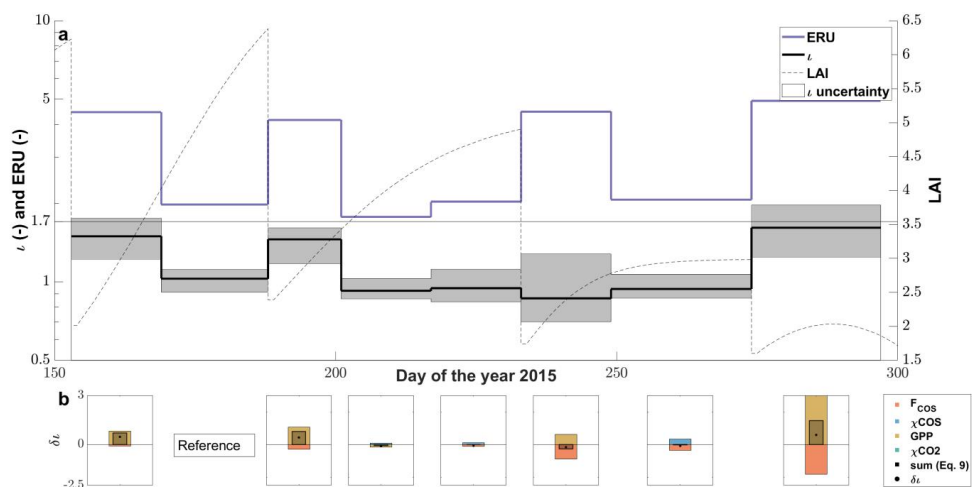
288



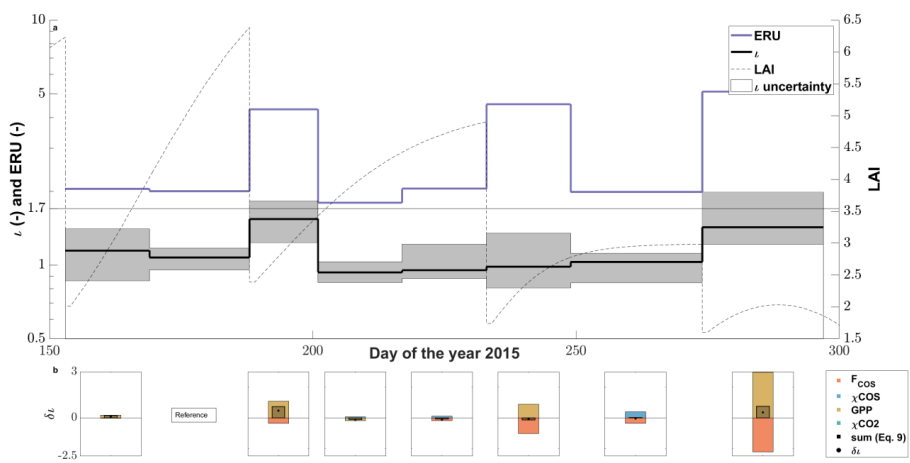
289

290

291 *New:*



292



293 *Old:*

294

295

## B. List of relevant changes

296

297

298

299

300

301

302

- The correct  $u^*$  filter is now applied and all values in the document have been changed accordingly
- During the reanalysis we were also able to recover more data from immediately after the first cut, which slightly increased LRU and ERU during this phase (Fig. 7a)
- The section about the COS and CO<sub>2</sub> mixing ratios is now placed before the flux sections in the result as well as the discussion section

303

## C. Tracked document

304

# 305 Seasonal dynamics of the COS and CO<sub>2</sub> exchange of a managed 306 temperate grassland

307 Felix M. Spielmann<sup>1</sup>, Albin Hammerle<sup>1</sup>, Florian Kitz<sup>1</sup>, Katharina Gerdel<sup>1</sup>, Georg Wohlfahrt<sup>1</sup>

308 <sup>1</sup>Department of Ecology, University of Innsbruck, Innsbruck, 6020, Austria

309 Correspondence to: Georg Wohlfahrt (Georg.Wohlfahrt@uibk.ac.at)

310 **Abstract.** Gross primary productivity (GPP), the CO<sub>2</sub> uptake by means of photosynthesis, cannot be measured directly on  
311 ecosystem scale, but has to be inferred from proxies or models. One newly emerged proxy is the trace gas carbonyl sulfide  
312 (COS). COS diffuses into plant leaves in a fashion very similar to CO<sub>2</sub>, but is generally not emitted by plants. Laboratory  
313 studies on leaf level gas exchange have shown promising correlations between the leaf relative uptake (LRU) of COS to CO<sub>2</sub>  
314 under controlled conditions. However, *in situ* measurements including daily to seasonal environmental changes are required,  
315 to test the applicability of COS as a tracer for GPP at larger temporal scales. To this end, we conducted concurrent  
316 ecosystem scale CO<sub>2</sub> and COS flux measurements above an agriculturally managed temperate mountain grassland. We also  
317 determined the magnitude and variability of the soil COS exchange, which can affect the LRU on ecosystem level. The  
318 cutting and removal of the grass at the site had a major influence on the soil [flux](#) as well as the total exchange of COS. The  
319 grassland acted as a major sink for CO<sub>2</sub> and COS during periods of high leaf area. The sink strength decreased after the cuts  
320 and the grassland turned into a net source for CO<sub>2</sub> and COS on ecosystem level. The soil acted as a small sink for COS when  
321 the canopy was undisturbed, but also turned into a source after the cuts, which we linked to higher incident radiation hitting  
322 the soil surface. However, the soil contribution was not large enough to explain the COS emission on ecosystem level,  
323 hinting to an unknown COS source possibly related to dead plant matter degradation. Over the course of the season, we  
324 observed a concurrent decrease of CO<sub>2</sub> and COS uptake on ecosystem level. With the exception of the short periods after the  
325 cuts, the LRU under high light conditions was rather stable and indicates a high correlation between the COS flux and GPP  
326 across the growing season.

327

## 328 1 Introduction

329 Carbonyl sulfide (COS) is the most abundant sulfur-containing gas in the atmosphere with tropospheric mixing ratios of  
330 ~500 ppt. Within the atmosphere, COS acts as a greenhouse gas with a 724 times higher direct radiative forcing efficiency as  
331 CO<sub>2</sub> (Brühl et al., 2012). After reaching the stratosphere, it reacts to sulfur aerosols via oxidation and photolysis, hence  
332 contributing to the backscattering of solar radiation and having a cooling effect on Earth's atmosphere (Krysztofiak et al.,  
333 2015; Whelan et al., 2018). The intra-seasonal atmospheric COS mixing ratio follows the pattern of CO<sub>2</sub> as terrestrial  
334 vegetation acts as the largest known sink for both species (Montzka et al., 2007; Whelan et al., 2018; Le Quere et al., 2018).  
335 However, [the relative decrease in ambient mixing ratio during summer of the northern hemisphere](#)~~the summer drawdown for~~  
336 [COS](#) is 6 times stronger [for COS](#) than for CO<sub>2</sub> (Montzka et al., 2007) as COS is generally not emitted by plants like CO<sub>2</sub>,  
337 which is released in respiration processes.

338 The uptake of COS by plants is mostly mediated by the enzyme carbonic anhydrase (CA), but also photolytic enzymes like  
339 Ribulose-1,5-bisphosphate-carboxylase/-oxygenase (Rubisco) (Lorimer and Pierce, 1989). This in turn means that COS and  
340 CO<sub>2</sub> share a similar pathway into leaves through the boundary layer, the stomata and the cytosol, up to their reaction sites.

341 Compared to CO<sub>2</sub>, COS is processed in a one-way reaction to H<sub>2</sub>S and CO<sub>2</sub> (Protoschill-Krebs and Kesselmeier, 1992;Notni  
342 et al., 2007) and therefore not released by plants, (with the exception of severely stressed plants (Bloem et al., 2012;Gimeno  
343 et al., 2017)). That makes COS an interesting tracer for estimating the stomatal conductance and the gross uptake of CO<sub>2</sub>,  
344 referred to as gross primary production (GPP), on ecosystem level (Asaf et al., 2013;Kooijmans et al., 2017;Kooijmans et al.,  
345 2019). However, to estimate GPP using COS, the relative uptake of COS to GPP deposition velocities (LRU) must be known  
346 beforehand (see Eq.1), so that GPP can be estimated on the basis of the COS flux.

$$347 \quad LRU = \frac{F_{COS}}{\chi_{COS}} \bigg/ \frac{F_{CO_2}}{\chi_{CO_2}} \quad (\text{Eq.1})$$

348 F<sub>COS</sub> is the COS leaf flux (pmol m<sup>-2</sup> s<sup>-1</sup>), F<sub>CO<sub>2</sub></sub> is the gross CO<sub>2</sub> uptake on leaf level (μmol m<sup>-2</sup> s<sup>-1</sup>) and χ<sub>COS</sub> and χ<sub>CO<sub>2</sub></sub> are the  
349 ambient COS and CO<sub>2</sub> mixing ratios in ppt and ppm, respectively. Leaf level studies for C<sub>3</sub> plants have estimated the LRU to  
350 be around 1.7 with the 95% confidence interval between 0.7 and 6.2 (Whelan et al., 2018;Seibt et al., 2010;Sandoval-Soto et  
351 al., 2005). The large spread of the LRU most likely originates from differences between plant species, for example, leaf  
352 structure and plant metabolism (Wohlfahrt et al., 2012;Seibt et al., 2010), which questions the applicability of the concept of  
353 LRU in real-world ecosystems under naturally varying environmental conditions. It is also known that the LRU is just stable  
354 under high light conditions, since the uptake of CO<sub>2</sub> by means of photosynthesis is a light driven process, while CA is able to  
355 process COS independently of light conditions (Maseyk et al., 2014;Yang et al., 2018;Stimmler et al., 2011). Any model of  
356 LRU should therefore reflect diurnal changes in light conditions. Kooijmans et al. (2019) recently discovered that the vapor  
357 pressure deficit (VPD) appears to have a stronger control on F<sub>COS</sub> than on F<sub>CO<sub>2</sub></sub>, in an evergreen needle forest. If generally  
358 true, this would add further variability to the LRU and complicating the application of COS to estimate GPP. Besides inter-  
359 specific differences in LRU, the question remains unanswered if the LRU is also susceptible to seasonal changes of  
360 ecosystems for example, changes in species composition or phenology, which would further complicate the application of  
361 COS in carbon cycle research. Maseyk et al. (2014) observed COS emissions on ecosystem scale over a winter wheat field  
362 going into senescence, indicating that potentially strong sources of COS could distort LRU.

363 Since CA and other enzymes known to emit or take up COS are also present in microorganisms (Ogawa et al., 2013;Seefeldt  
364 et al., 1995;Ensign, 1995;Smeulders et al., 2013;Whelan et al., 2018), recent studies have also quantified the contribution of  
365 soils to the COS ecosystem flux (Kooijmans et al., 2017;Spielmann et al., 2019;Maseyk et al., 2014). COS soil fluxes could  
366 modify the LRU on ecosystem level and hence inferred GPP, if they are substantial compared to COS canopy fluxes. Similar  
367 to the ecosystem fluxes, the soil fluxes could not only be prone to diurnal, but also seasonal changes, depending on the  
368 substrate availability, environmental conditions (e.g. soil temperature and moisture), substrate quality and quantity, and  
369 changes in composition of the microbial communities (Kitz et al., 2019;Meredith et al., 2019). Recent studies have also  
370 linked COS soil emissions to abiotic processes dependent on light and/or temperature (Whelan and Rhew, 2015;Kitz et al.,  
371 2019;Meredith et al., 2018).

372 The goal of our study was to provide new insights into the seasonal variability of COS fluxes on ecosystem, soil and canopy  
373 level. To this end, we conducted a 6-month campaign on a managed temperate mountain grassland, measuring ecosystem as  
374 well as soil COS fluxes. Since the grassland was cut four times during the campaign, we were able to observe multiple  
375 growing cycles and investigate the diel and seasonal changes of the COS fluxes and the LRU in this highly dynamic  
376 ecosystem. We hypothesize that (H1) the grassland, given its large CO<sub>2</sub> uptake capacity (Wohlfahrt et al. 2008), is a major  
377 sink for COS and that the sink strength decreases over the course of the season, (H2) the drying of the cut grass leads to a  
378 release of COS, (H3) the LRU will change after the cuts, due to stressed plants and drying plant parts in the field, but is  
379 otherwise stable, (H4) the cuts turn the soil into a COS source, due to the larger amount of light reaching the soil surface  
380 (Kitz et al., 2017), but once a reasonably high leaf area index (LAI) has developed, COS is taken up by soil.

## 381 2 Methods

### 382 2.1 Study site and period

383 The study was conducted at an intensively managed mountain grassland in the municipal territory of Neustift (Austria) in  
384 Stubai valley (FLUXNET ID: AT-Neu; doi: [10.18140/FLX/1440121](https://doi.org/10.18140/FLX/1440121)). The grassland is situated at an elevation of 970 m a.s.l.  
385 in the middle of the flat valley bottom. The soil was classified as Fluvisol with an estimated depth of 1 m with the majority  
386 of roots located within the first 10 cm. Measurements were conducted between 01.05.2015 and 31.10.2015 (183 days). The  
387 vegetation was described as Pastincao-Arrhenatheretum and consisted mainly of *Dactylis glomerata*, *Festuca pratensis*,  
388 *Alopecurus pratensis*, *Trisetum flavescens*, *Ranunculus acris*, *Taraxacum officinale*, *Trifolium repens*, *Trifolium pratense*,  
389 and *Carum carvi* (Kitz et al., 2017). During the campaign, the grassland was cut four times (02.06./07.07./21.08./01.10.2015)  
390 and the biomass left to dry on the field for up to one day, before being removed as silage. [Each year, the field site was](#)  
391 [fertilized with organic-solid manure and cattle slurry](#) (Hörtnagl et al., 2018) [at the end of the season \(07.10. in 2015\)](#).

### 392 2.2 Leaf area index

393 The LAI was estimated from assessments of the average canopy height, which were related to destructive LAI  
394 measurements, using the following sigmoid function:

$$395 \text{LAI} = \frac{1}{(1 + \exp(-(a_1 \text{DOY} + a_2)))} (b_1 - b_2) \quad (\text{Eq.2})$$

396 where DOY is the day of the year and a1, a2, b1 and b2 are factors that were optimized for each growing period, for  
397 example, before the first cut, between cuts and after fourth cut (Wohlfahrt et al., 2008). Additionally, biomass samples were  
398 taken at 15 occasions, to assist with the LAI calculation.

### 399 2.3 Mixing ratio measurements

400 The CO<sub>2</sub> ( $\chi_{\text{CO}_2}$ ) and COS ( $\chi_{\text{COS}}$ ) mixing ratios were measured using a Quantum Cascade Laser (QCL) Mini Monitor  
401 (Aerodyne Research, Billerica, MA, USA) at a wavenumber of ca. 2056 cm<sup>-1</sup> and at a frequency of 10 Hz. To minimize the  
402 effect of air temperature ( $T_{\text{air}}$ ) changes on the instrument, we placed it in an insulated box which in turn was located in a  
403 climate controlled instrument hut (30°C). The cooling of the laser was achieved by a chiller (ThermoCube 400, Solid State  
404 Cooling Systems, Wappinger Falls, NY, USA).

405 We used ¼ inch Teflon™ tubing, stainless steel fittings (SWAGELOK, Solon, OH, USA and FITOK, Offenbach, HE,  
406 Germany), Teflon Filters (Savilex, EdenPrarie, MN, USA) as well as COS-inert valves (Parker-Hannafin, Cleveland, OH,  
407 USA) to ensure that only materials known not to interact with COS were used for the measurement and calibration airflow.

408 ~~The H<sub>2</sub>O and CO<sub>2</sub> mixing ratios ( $\chi_{\text{H}_2\text{O}}$  &  $\chi_{\text{CO}_2}$ ) were measured by a closed path infrared gas analyzer (IRGA) (Licor 6262,~~  
409 ~~LICOR Biosciences, Lincoln, NE, USA). Since the data of the QCL, and the sonic anemometer and the IRGA were saved~~  
410 ~~on two separate PCs, a network time protocol software (NTP, Meinberg, NI, Germany) was used to keep the time on both~~  
411 ~~devices synchronized. We corrected known  $\chi_{\text{COS}}$  drift issues of the QCL (Kooijmans et al., 2016) by doing half hourly~~  
412 ~~calibrations for 1 min with a gas of known  $\chi_{\text{COS}}$ . The gas cylinders (working standards) used for the calibrations were either~~  
413 ~~pressurized air (UN 1002) or nitrogen (UN 1066), which were cross-compared (when working standard cylinders were full~~  
414 ~~and close to empty) to an Aculife-treated aluminum pressurized air cylinder obtained from the National Oceanic &~~  
415 ~~Atmospheric Administration (NOAA). The latter was analyzed by the central calibration laboratory of NOAA for its  $\chi_{\text{COS}}$~~   
416 ~~using gas chromatography with mass spectrometric detection (GC-MS) on 06.04.2015. We then linearly interpolated~~  
417 ~~between the offsets of the half hourly calibrations and used the retrieved values to correct the high frequency COS data. Due~~  
418 ~~to issues with the scale gas cylinder, no absolute concentrations were available before the 16.06. first cut. The COS mixing~~  
419 ~~ratios were extrapolated to the 1<sup>st</sup> cut to increase the amount of available data for the first post cut and therefore no LRU was~~

420 | ~~calculated for this~~ period. This was done on the basis of the measured CO<sub>2</sub> mixing ratios and the mean half hourly ratio of  
421 | the ambient CO<sub>2</sub> to COS mixing ratios between the 16. and the 18.6..

### 422 **2.3.1 Mixing ratio measurements within the canopy**

423 In order to investigate the  $\chi_{\text{COS}}$  within the canopy, we used a multiplexer and 8 ¼ inch Teflon™ tubes to measure the  $\chi_{\text{COS}}$  at  
424 8 heights within and above the canopy i.e. at 2, 5, 10, 20, 30, 40, 50 & 250 cm height above ground with a tube length of  
425 15 m for each height. The upper two intakes were located at the eddy covariance measurement and canopy height,  
426 respectively. Each height was measured for 1 min at 1 Hz and 2 l min<sup>-1</sup>, while the other lines were each flushed at 2 l min<sup>-1</sup>.  
427 The  $\chi_{\text{COS}}$  drift was also corrected by doing half hourly calibrations (see section 2.3).  
428

## 429 **2.4 COS soil fluxes**

### 430 **2.4.1 Soil chamber setup**

431 To quantify soil COS fluxes, we installed four stainless steel (SAE grade: 316L) rings 5 cm into the soil. They remained on  
432 site for 112 days (10.06.2015 – 30.09.2015). Two additional rings were installed on the 31.08.2015 and the 02.10.2015 to  
433 examine any long-term effects of the ring placement and to replace the original rings for the measurements in September and  
434 | October. The aboveground biomass within each ring was removed at the day of installation and again at least one day prior  
435 to each measurement day. The roots within as well as the vegetation surrounding the rings were not removed and natural  
436 litter was left in place. At days without measurements the soil within the rings was covered by fleece to prevent it from  
437 drying out.

438 To measure the soil fluxes, a transparent fused silica-glass chamber (Kitz et al., 2017) was placed into the water filled  
439 channel of the steel rings, while air was sucked through the chamber to the QCL at a flow rate of 1.5 l min<sup>-1</sup>. The chamber  
440  $\chi_{\text{COS}}$  was then compared with the ambient  $\chi_{\text{COS}}$  above the chamber, using a second inlet to which we switched before the  
441 | chamber measurement and after reaching stable readings inside the chamber. The intake height of the ambient as well as the  
442 | inlet of the chamber air were located at 0.12 m above the ground and thus within the canopy height with the exception of  
443 | measurements right after the cuts (see cutting dates in Section 2.1). Overall, 243 chamber measurements were conducted  
444 over the course of the campaign including day and nighttime measurements. Additional manual measurements included a  
445 hand-held sensor (WET-2, Delta-T Devices, Cambridge, England) to measure soil water content (SWC) and soil temperature  
446 ( $T_{\text{soil}}$ ) at a soil depth of 5 cm simultaneously with the soil chamber measurements next to the rings.

### 447 **2.4.1 COS soil flux calculation**

448 The COS soil flux was calculated using the following equation:

$$449 \quad F = q(\chi_{\text{COS}2} - \chi_{\text{COS}1})/A \quad (\text{Eq.3})$$

450 where F is the COS soil flux (pmol m<sup>-2</sup> s<sup>-1</sup>), q denotes the flowrate in (mol s<sup>-1</sup>),  $\chi_{\text{COS}2}$  and  $\chi_{\text{COS}1}$  are the chamber and ambient  
451  $\chi_{\text{COS}}$  in ppt, respectively and A the soil surface area (0.032 m<sup>2</sup>) covered by the chamber. A more detailed description can be  
452 found in Kitz et al. (2017).

### 453 **2.4.2 COS soil exchange modelling**

454 Due to the removal of the aboveground biomass and the consequent higher shortwave radiation reaching the soil surface in  
455 the chambers, compared to the soil below the canopy, we simulated the soil COS exchange for natural conditions. The soil  
456 flux was modelled using our measured soil fluxes and additionally retrieved soil and meteorological data -  $T_{\text{soil}}$ , soil water  
457 content (SWC) at 5 cm depth next to the chambers and incident shortwave radiation reaching the soil surface ( $R_{\text{SW-soil}}$ ) - as



458 input for a random forest regression model (Liaw and Wiener, 2002). The soil fluxes were modelled on half hourly basis for  
459 the whole duration of the measurement campaign to calculate the COS canopy fluxes from the difference of the COS  
460 ecosystem and soil fluxes. To this end we used the scikit-learn (sklearn Ver. 0.19.1) package, the pandas library and the  
461 Python Software Distribution Anaconda (Ver. 5.2.0) in the command shell Ipython (Ver. 6.4.0) based on the Programming  
462 language Python (Ver. 3.3.5). We used the Beer-Lambert law to model  $R_{SW\_soil}$  under undisturbed conditions as the  
463 aboveground vegetation was removed to measure the COS exchange of bare soil:

$$464 \quad R_{SW\_soil} = R_{SW} \exp(-K LAI) \quad (\text{Eq.4})$$

465 where  $R_{SW\_soil}$  ( $\text{Wm}^{-2}\text{s}^{-1}$ ) is the shortwave radiation (SW) reaching the soil surface,  $R_{SW}$  is the incoming SW radiation  
466 reaching the top of the canopy, LAI is the plant area index (Eq. 2) and K is the canopy extinction coefficient assuming a  
467 spherical leaf inclination distribution (Wohlfahrt et al., 2001), which was calculated using the following equation:

$$468 \quad K = \frac{1}{2\cos(\psi)} \quad (\text{Eq.5})$$

469 where  $\psi$  is the zenith angle of the sun in radians.

470

471 A random forest with 1000 trees was grown which resulted in an out of bag (OOB) score of (0.82). The OOB score can be  
472 interpreted as a pseudo-R2 and is widely used in random forest analyses (regression and classification), especially in the  
473 absence of a proper test dataset. It uses the data not seen by the trees (random forest uses bootstrapping) as a test dataset. The  
474 optimal input parameters, including maximum tree depth, were determined with the function GridSearchCV from the sklearn  
475 package.

## 476 2.5 Ecosystem fluxes

### 477 2.5.1 Setup for ecosystem fluxes

478 The COS, CO<sub>2</sub> and H<sub>2</sub>O ecosystem fluxes were obtained using the eddy covariance method (Aubinet et al., 1999; Baldocchi,  
479 2014). We used a 3-axis sonic anemometer (Gill R3IA, Gill Instruments Limited, Lymington, UK) to obtain high-high-  
480 resolution data of the 3 wind components. The intake of the tube for the eddy covariance measurements was installed in  
481 close proximity to the sonic anemometer and insulated as well as heated above  $T_{air}$  to prevent condensation within the tube.  
482 The air was sucked to the QCL at a flowrate of  $7 \text{ l min}^{-1}$  using a Vacuum Pump (Agilent Technologies, CA, USA).

### 483 2.5.2 Ecosystem flux calculation

484 In a first step we used a self-developed software to determine the time lag, introduced by the separation of tube intake and  
485 the sonic anemometer and the tube length, between the QCL and sonic dataset (Hortnagl et al., 2010). The data were then  
486 processed using the software EdiRe (University of Edinburgh, UK) and Matlab2019a (MathWorks, MA, USA). We used the  
487 laser drift corrected  $\chi_{COS}$  data and linear detrending to process the data before following the procedure to correct for sensor  
488 response, tube attenuation, path averaging and sensor separation following Gerdel et al. (2017). The random flux uncertainty  
489 was calculated following Langford et al. (2015).

490 We estimated the COS canopy flux from the difference between the measured COS ecosystem and the modelled COS soil  
491 flux.

### 492 2.5.3 Flux partitioning and leaf relative uptake

493 The GPP on ecosystem level was determined using the FP+ model put forward by Spielmann et al. (2019). The model  
494 estimates the GPP on the basis of nighttime net ecosystem exchange (NEE) measurements of CO<sub>2</sub> that are assumed to  
495 provide the temperature response of the ecosystem respiration (RECO) as well as a light dependency curve to estimate GPP  
496 based on the daytime NEE (Lasslop et al., 2010):

497 
$$NEE = \frac{\alpha \beta R_{PAR}}{\alpha R_{PAR} + \beta} + r b e^{E_0 \left( \frac{1}{T_{ref} - T_0} - \frac{1}{T_{air} - T_0} \right)}$$
 (Eq.6)

498 where  $\alpha$  denotes the canopy light utilization efficiency ( $\mu\text{mol CO}_2 \mu\text{mol}^{-1}$  photons),  $\beta$  the maximum  $\text{CO}_2$  uptake rate of the  
 499 canopy at light saturation ( $\mu\text{mol CO}_2 \text{m}^{-2} \text{s}^{-1}$ ),  $R_{PAR}$  the incoming photosynthetic active radiation ( $\mu\text{mol m}^{-2} \text{s}^{-1}$ ),  $rb$  the  
 500 ecosystem base respiration ( $\mu\text{mol m}^{-2} \text{s}^{-1}$ ) at the reference temperature  $T_{ref}$  ( $^{\circ}\text{C}$ ), which is set to  $15^{\circ}\text{C}$ ,  $T_{air}$  ( $^{\circ}\text{C}$ ) refers to the  
 501 air temperature and  $E_0$  ( $^{\circ}\text{C}$ ) to the temperature sensitivity of RECO.  $T_0$  was kept constant at  $-46.02^{\circ}\text{C}$ . We did not use the  
 502 VPD modifier of beta put forward by Lasslop et al. (2010) as its value could not be estimated with confidence. We  
 503 determined the parameter  $E_0$  by using nighttime data minimizing the root squared mean error. For the determination of the  
 504 remaining five unknown model parameters of the two flux partitioning models we used DREAM, a multi-chain Markov  
 505 Chain Monte Carlo algorithm (for more detail see Spielmann et al. (2019)). We calculated the parameters for ~15 day  
 506 windows but adjusted them to not overlap with a cut of the grassland.  
 507 The ecosystem relative uptake (ERU) was calculated using Eq. 1 substituting the GPP with the NEE and using the COS  
 508 ecosystem flux for  $F_{COS}$ .

509 The FP+ model by Spielmann et al. (2019) extends the daytime FP (Eq.6) to also estimate the COS ecosystem fluxes by  
 510 linking the GPP resulting from the first part on the right-hand side of Eq.6 with the COS exchange through:

511 
$$F_{COSmodel} = \frac{\frac{GPP \cdot LRU}{\chi_{CO_2}}}{\frac{\chi_{COS}}{\chi_{CO_2}}} = \frac{GPP \cdot LRU \cdot \chi_{COS}}{\chi_{CO_2}}$$
 (Eq.7)

512 developed by Sandoval-Soto et al. (2005). where  $F_{COSmodel}$  is the modelled COS flux ( $\text{pmol m}^{-2} \text{s}^{-1}$ , (ppt) and  $\chi_{CO_2}$  (ppm)  
 513 are the measured ambient mixing ratios of COS and  $\text{CO}_2$  respectively and LRU (-) is the leaf relative uptake rate:

514 
$$LRU = \iota e^{\left( \frac{\kappa}{R_{PAR}} \right)}$$
 (Eq.8)

515 where  $\iota$  (-) corresponds to the LRU at high light intensity and the parameter  $\kappa$  ( $\mu\text{mol m}^{-2} \text{s}^{-1}$ ) governs the increase of LRU at  
 516 low light conditions. While mathematically  $\iota$  is only obtained at infinitely high PAR, in practice above about  $700 \mu\text{mol m}^{-2} \text{s}^{-1}$   
 517  $\iota$  PAR (Kooijmans et al., 2019) only insignificant change is reported in other studies (Stimler et al., 2011). The light  
 518 dependency of LRU originates from the fact that the COS uptake by the enzyme CA is light-independent, while the  $\text{CO}_2$   
 519 uptake by Rubisco depends on solar radiation absorbed by leaf chlorophyll (Whelan et al., 2018; Kooijmans et al.,  
 520 2019; Wohlfahrt et al., 2012).

521 The method stated above infers LRU solely on the basis of ecosystem scale fluxes, whereas other studies typically use  
 522 branch/leaf chamber measurements (Yang et al., 2018) to determine the relationship between the COS and  $\text{CO}_2$  uptake  
 523 rates. We determined the parameter  $E_0$  by using nighttime data minimizing the root squared mean error. For the determination  
 524 of the remaining five unknown model parameters of the two flux partitioning models we used DREAM, a multi chain  
 525 Markov Chain Monte Carlo algorithm (for more detail see Spielmann et al. (2019)). We calculated the parameters for ~15  
 526 day windows but adjusted them to not overlap with a cut of the grassland.  
 527 The ecosystem relative uptake (ERU) was calculated using Eq. 1 substituting the GPP with the NEE and using the COS  
 528 ecosystem flux for  $F_{COS}$ .

#### 529 2.5.4 Linear perturbation analysis

530 The relative contribution of the parameters GPP,  $F_{COSmodel}$ ,  $\chi_{CO_2}$  and  $\chi_{COS}$  that drive  $\iota$  (Eq. 7) were estimated through a linear  
 531 perturbation analysis (Stoy et al., 2006).

532 The changes in  $\iota$  ( $\delta\iota$ ) between the target and the reference window (before the 2<sup>nd</sup> cut, i.e. 18.06.2015-07.07.2015) are  
 533 considered the total derivative of Eq. 7 and can be represented by a multivariate Taylors's expansion where the higher-order  
 534 terms are neglected in this first-order analysis:

535 
$$\delta\iota = \frac{\partial\iota}{\partial F_{COSmod}} dF_{COSmod} + \frac{\partial\iota}{\partial\chi_{COS}} d\chi_{COS} + \frac{\partial\iota}{\partial GPP} dGPP + \frac{\partial\iota}{\partial\chi_{CO_2}} d\chi_{CO_2}$$
 (Eq.9)

Formatiert: Hochgestellt

Formatiert: Hochgestellt

536 The relative contributions of the parameters were determined by computing the partial derivatives of Eq. 7.

$$537 \frac{\partial I}{\partial F_{COSmod}} = \frac{\chi_{CO2}}{\chi_{COS}GPP} \quad (\text{Eq.10})$$

$$538 \frac{\partial I}{\partial \chi_{COS}} = \frac{-\chi_{CO2}F_{COSmod}}{\chi_{COS}^2GPP} \quad (\text{Eq.11})$$

$$539 \frac{\partial I}{\partial GPP} = \frac{\chi_{CO2}F_{COSmod}}{\chi_{COS}GPP^2} \quad (\text{Eq.12})$$

$$540 \frac{\partial I}{\partial \chi_{CO2}} = \frac{F_{COSmod}}{\chi_{COS}GPP} \quad (\text{Eq.13})$$

541

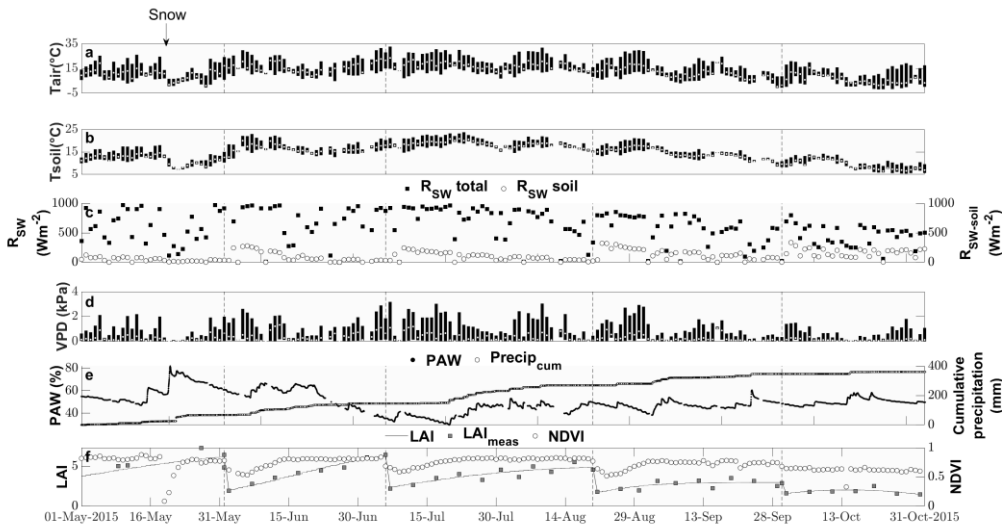
## 542 2.6 Ancillary data

543 Supporting meteorological measurements included  $T_{air}$  (RFT-2, UMS, Munich, GER),  $T_{soil}$  (TCAV, Campbell Scientific,  
544 Logan, UT, USA), SWC (ML2x, Delta-T Devices, Cambridge, UK), incident solar radiation (CNR-1, Klipp and Zonen,  
545 Delft, NLD), incident photosynthetic active radiation (PAR) (BF2H, Delta-T Devices Ltd, Cambridge, UK) and the  
546 Normalized Difference Vegetation Index (NDVI) sensor (SRS-NDVI, Meter, Pullman, WA, USA). The data were recorded  
547 throughout the whole season as 1 min values and stored as half-hourly means and standard deviations.

## 548 3 Results

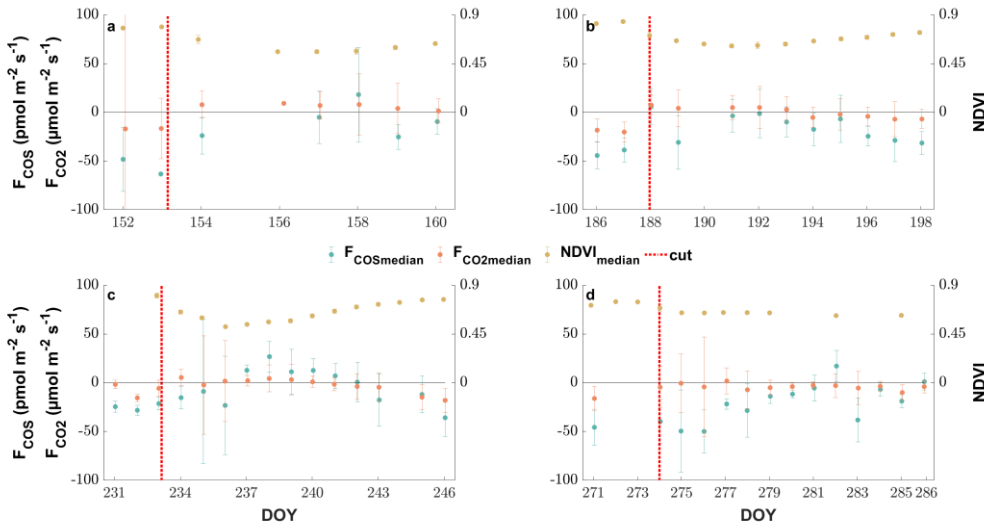
### 549 3.1 Environmental conditions

550 Air temperature ranged between  $-2\text{ }^{\circ}\text{C}$  and  $33\text{ }^{\circ}\text{C}$  with a mean of  $13\text{ }^{\circ}\text{C}$  during the study period from 15<sup>th</sup> of May to first of  
551 November (Fig. 1). While the majority of precipitation (total 360.5 mm) fell as rain, we observed an exceptionally late snow  
552 event on the 20<sup>th</sup> of May, which did not melt for almost two days (Fig. 1). Although the VPD reached values of above 2 kPa  
553 during 25 days, and plant available water dropped below 38-50 % on 21-111 days during the campaign (Fig. 1), we did not  
554 observe any relationship with COS (see Fig S1-S2). Due to the removal of the aboveground biomass, the cuts reduced LAI.  
555 They also reduced the normalized difference vegetation index (NDVI) (Fig. 1), which is a measure of canopy greenness  
556 (Tucker, 1979), which The NDVI further decreased in the subsequent days as a consequence of dying plant parts remaining at  
557 the field site (Fig 2 panels a-c). This can also be observed in the webcam photos (**Photo S1-S3**).



558

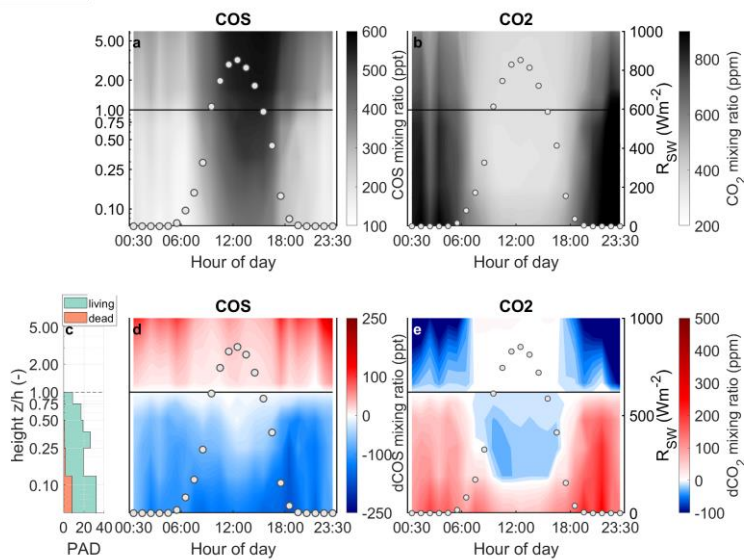
559 **Figure 1.** Seasonal cycle of ancillary variables. Daily minimum, maximum and median (a) air and (b) soil temperatures (°C) indicated by  
 560 the lower and upper end of the bars and the white circle, respectively. (c) Daily maximum incident ~~photosynthetic active~~  
 561 ~~radiation~~ ~~shortwave radiation~~ ( $\mu\text{mol W m}^{-2} \text{s}^{-1}$ ) reaching the top of the canopy (black squares) and reaching the soil surface (white circles).  
 562 (d) Daily minimum, maximum and median vapor pressure deficit (kPA) indicated by the lower and upper end of the bars and the white  
 563 circle, respectively. (e) ~~Soil water content~~ ~~Plant available water~~ (%) depicted by black squares and cumulative precipitation (mm) depicted  
 564 by open circles. (f) Modelled leaf area index (black lines), measured LAI (grey squares) and normalized difference vegetation index (open  
 565 circles).



566  
 567 **Figure 2:** The response of the daily midday medians of NDVI (yellow circles), COS (blue circles) and CO<sub>2</sub> (red circles) ecosystem fluxes  
 568 around the 4 cutting events (a-d) of the grassland. The errorbars depict the respective median absolute deviations. The cuts are marked by a  
 569 red dashed line.

570 **3.2 COS mixing ratios above and within the canopy**

571 While the canopy depleted the ambient  $\chi_{\text{COS}}$  during day as well as nighttime, we found that the  $\chi_{\text{COS}}$  reached values as low as  
 572 134 ppt (depletion of 102 ppt with respect to the mixing ratio at canopy height) during nighttime (see Fig. 3) at the bottom of  
 573 the canopy in contrast to the midday  $\chi_{\text{COS}}$ , which only went down to 389 ppt (depletion of 125 ppt with respect to the mixing  
 574 ratio at canopy height). We observed a decrease in  $\chi_{\text{CO}_2}$  (up to 26 ppm) within the most upper layers of the canopy compared  
 575 to  $\chi_{\text{CO}_2}$  at canopy height during daytime, while  $\chi_{\text{CO}_2}$  increased within the lowest layers compared to  $\chi_{\text{CO}_2}$  at the canopy height  
 576 due to soil respiration. The above canopy  $\chi_{\text{COS}}$  increased considerably starting at the onset of the day and reached 587 ppt at  
 577 4 p.m. with a steep increase until 11 a.m. Over the course of the season the midday ambient  $\chi_{\text{COS}}$  decreased from  $500 \pm 28$  ppt  
 578 from mid-June to mid-July to  $405 \pm 29$  ppt in October with the trend of increasing  $\chi_{\text{COS}}$  starting at the end of September (see  
 579 Fig. S6).



580

581 **Figure 3.** Vertical gradient of the (a) COS and (b) CO<sub>2</sub> mixing ratio (ppt and ppm, respectively) depicted by the background color between  
 582 the soil and the eddy covariance tower at 250 cm for one day. The left y axis shows the log of the measurement divided by the canopy  
 583 height (z/h). The white circles depict the incoming shortwave radiation (R<sub>SW</sub>) in (W m<sup>-2</sup>). Plant area density (PAD) split into living (green)  
 584 and dead (brown) plant material (c). Vertical gradient of the difference between the mixing ratio at canopy height and each measurement  
 585 height for (d) COS and (e) CO<sub>2</sub>.

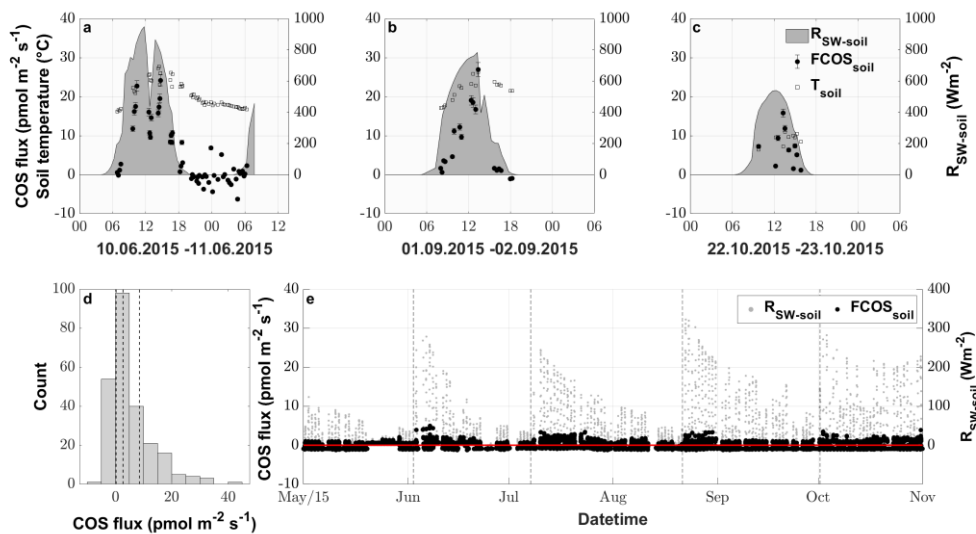
586

### 587 3.2.3 COS soil flux

588 The fluxes resulting from the soil chamber measurements ranged from -6.3 to 40.9 pmol m<sup>-2</sup>s<sup>-1</sup>, with positive fluxes denoting  
 589 emission (see Fig. 3-4 panel d).

590 During nighttime (R<sub>SW</sub> = 0, n = 43), 74.4 % of the COS fluxes were negative, implying that the soil of the grassland acted  
 591 as a net sink for COS. During nighttime (R<sub>SW</sub> = 0, n = 43), the soils of the grassland acted as a net sink for COS 74.4 % of the  
 592 time (range of -4.4 to 6.9 pmol m<sup>-2</sup>s<sup>-1</sup>), whereas soils transitioned to a source in 88.5 % of all daytime measurements (R<sub>SW</sub> >  
 593 0, n = 200), reaching the highest fluxes of 40.9 pmol m<sup>-2</sup>s<sup>-1</sup> during midday (see Fig. 3-4 a-c and Fig. S3). This diel pattern  
 594 was maintained over the course of the season, however with decreasing maximum COS source strength of the soil towards  
 595 the end of the season (Fig. 3-4 a-c and Fig. S3). The random forest regression revealed that the most important variable for  
 596 predicting the soil fluxes was the incident shortwave radiation reaching the soil surface (R<sub>SW-soil</sub>), accounting for more than  
 597 73.53 % of the total variance explained by the final model, while SWC and T<sub>soil</sub> only accounted for 17.84 % and 8.62 %,   
 598 respectively. The fast response of the COS soil fluxes to changes in R<sub>SW</sub> can be seen in Fig. 3-4 a, where we observed a  
 599 decrease of R<sub>SW-soil</sub> as well as the COS soil flux during a cloudy period, even when the soil temperature still increased. Soil  
 600 fluxes estimated with the random forest regression ranged from -1.3 to 5.0 pmol m<sup>-2</sup>s<sup>-1</sup>, reflecting the fact that under real-  
 601 world conditions very little solar radiation reaches the soil surface. (Fig. 3-4 e). The resulting emissions peaked during  
 602 daytime shortly after the cuts when a high proportion of incident radiation was reaching the soil surface, while simulated  
 603 nighttime fluxes were dominated by uptake (in 93 % of all cases) for the whole season.

604



605

606 **Figure 43.** COS soil fluxes ( $\text{pmol m}^{-2}\text{s}^{-1}$ ) originating from manual chamber measurements of three selected days (a), (b) and (c) depicted  
 607 by black circles and open diamonds, respectively, incident shortwave radiation reaching the soil ( $R_{\text{SW-soil}}$ ) depicted by the gray area and  
 608 soil temperature ( $T_{\text{soil}}$ ) depicted by empty black bordered squares. (d) Histogram of all conducted COS soil chamber observations with the  
 609 dashed vertical lines depicting the 25, 50 and 75% quantile. (e) Season plot of the modelled COS soil fluxes ( $F_{\text{COSsoil}}$ ) depicted by the black  
 610 circles, incident shortwave radiation reaching the soil surface ( $R_{\text{SW-soil}}$ ) depicted by grey circles and the black dashed lines depicting the  
 611 cuttings of the grassland.

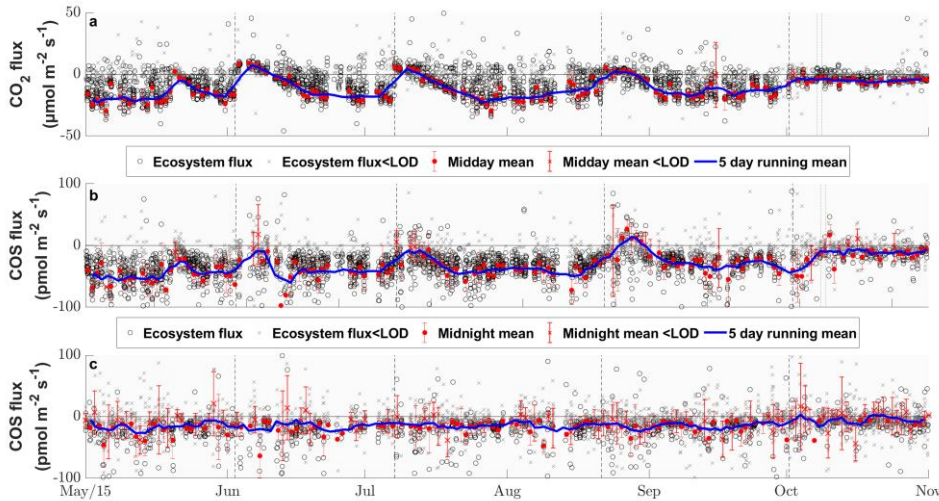
612

### 613 3.3.4 COS and CO<sub>2</sub> ecosystem-scale fluxes

614 The grassland acted as a net sink for COS during the majority of our study period with 80 % of the COS ecosystem fluxes  
 615 between  $-60.2$ – $56.0$   $\text{pmol m}^{-2}\text{s}^{-1}$  and  $-12.5$ – $4.5$   $\text{pmol m}^{-2}\text{s}^{-1}$  during daytime and  $-41.5$ – $37.8$   $\text{pmol m}^{-2}\text{s}^{-1}$  and  $-4.6$ – $9.2$   $\text{pmol m}^{-2}\text{s}^{-1}$   
 616 during nighttime. However, we also observed a net release of COS at the field site 4.5–11.2 % of the time. The net CO<sub>2</sub>  
 617 fluxes ranged from  $-20.7$ – $4$   $\mu\text{mol m}^{-2}\text{s}^{-1}$  and  $4.6$ – $30.3$   $\mu\text{mol m}^{-2}\text{s}^{-1}$  to  $28.7$ – $36.4$   $\mu\text{mol m}^{-2}\text{s}^{-1}$  for 80% of all observation during day  
 618 and nighttime, with daytime net emissions occurring after the cuttings of the grassland (Fig. 2 a-c and Fig. 4-5 a). While the  
 619 COS nighttime fluxes remained unaffected by the cuts (Fig. 4-5 c), the daytime fluxes showed a high variability (see Fig. 4-5  
 620 b). Especially after the cuts we observed a strong decline in COS uptake (Fig. 4 b) and the grassland even turned into a net  
 621 source for COS in middays (Fig. 2 a-c) with a highest emission flux of  $26.8$   $\text{pmol m}^{-2}\text{s}^{-1}$  (midday median) in August after the  
 622 cut. Especially after the cuts we observed a strong decline in COS uptake and even times where the grassland turned into a  
 623 net source for COS with midday means of up to  $24.5$   $\text{pmol m}^{-2}\text{s}^{-1}$  (Fig. 4 b). We observed COS emissions for up to 8 days  
 624 after the cut, when the dried litter had already been removed (Fig. 2 a-c). Compared to respiration processes outpacing GPP  
 625 almost instantaneously after the cuts, the grassland reached its peak COS emission on the day of the cut only in July,  
 626 whereas the peak was reached five days after the cut in June and August (Fig. 2 a-c). The cut in October led to a reduction in  
 627 COS uptake, which declined across several days and did not recover, as the end of the season was reached (Fig. 2 d & Fig. 5  
 628 b). The cut in October led to a reduction in COS uptake, which was lowest three days after the cut (Fig. 2 d). After the  
 629 fertilization of the field in October the grassland also turned into a source for COS during midday hours for one day (Fig. 4-5  
 630 b). Our flux measurements also included a time when the grassland was covered with snow (on the 20.05.2015), which  
 631 reduced the COS (and CO<sub>2</sub>) fluxes to values close to zero. Over the course of the season, we observed a decline in the  
 632 magnitude of the daytime COS uptake from  $-50.69 \pm 25.24$ – $0.6$   $\text{pmol m}^{-2}\text{s}^{-1}$  during midday in the first week of May down to -  
 633  $29.6$ – $10.3 \pm 25.5$ – $10.4$   $\text{pmol m}^{-2}\text{s}^{-1}$  in the last week of October, which was also correlated with the decline in the CO<sub>2</sub> sink

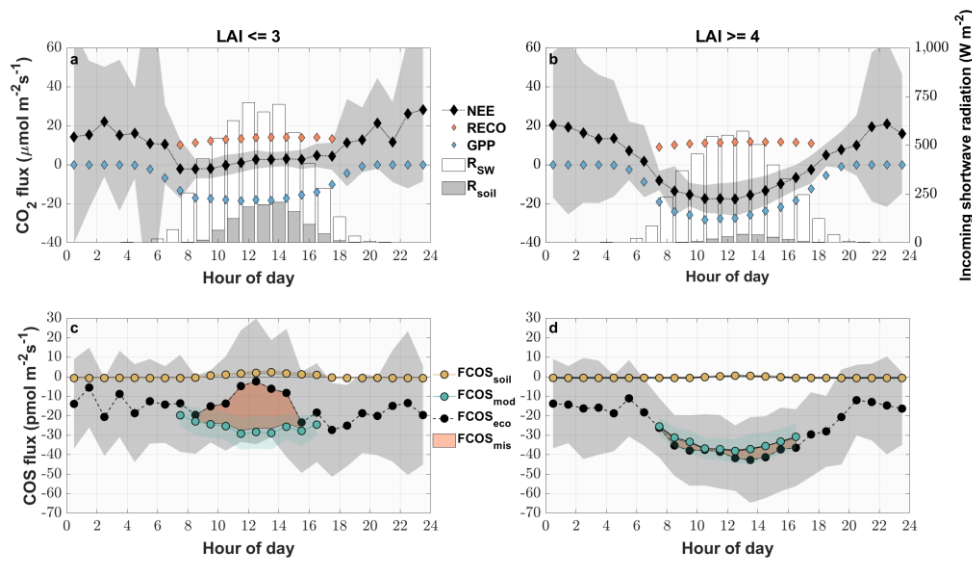


634 strength and shift to net emission of CO<sub>2</sub> from  $-19.9 \pm 8.0 \mu\text{mol m}^{-2}\text{s}^{-1}$  to  $11.9-4.4 \pm 36.91.5 \mu\text{mol m}^{-2}\text{s}^{-1}$  (Fig. 4-5 a-eb). We  
 635 observed an increase in COS and CO<sub>2</sub> fluxes within the growing phases after the cuts only up to an LAI of  $\sim 4$  (-) (Fig. S4-  
 636 S5), which then levelled out for COS and declined for CO<sub>2</sub> due to ecosystem respiration compensating GPP.



637  
 638 **Figure 45:** Seasonal cycle of the half hourly CO<sub>2</sub> (a), COS daytime (b) and COS nighttime (c) ecosystem fluxes in  $\mu\text{mol m}^{-2}\text{s}^{-1}$  and  $\text{pmol m}^{-2}\text{s}^{-1}$   
 639  $\text{m}^{-2}\text{s}^{-1}$  depicted by black circles if they are above the limit of detection (LOD) and grey x's if they are below (Langford et al., 2015). The  
 640 red circles depict the mean fluxes between 11 a.m. and 2 p.m. CET for (a & b) and between 11 p.m. and 2 a.m. for (c) that are above the  
 641 LOD, while the red x's indicate means below the LOD. The red error bars depict the  $\pm 1$  standard deviation of the mean. The blue lines  
 642 depict the running mean (5 days) for the mean fluxes. The black dashed lines depict the cuttings of the grassland.

643  
 644 The seasonal pattern of a decrease in COS sink strength was similar for nighttime fluxes ( $-18.40 \pm 29.76 \text{ pmol m}^{-2}\text{s}^{-1}$  to -  
 645  $13.010.6 \pm 22.518.2 \text{ pmol m}^{-2}\text{s}^{-1}$ ) (Fig. 4a5c). The mean nighttime respiration also decreased over the course of the season  
 646 from  $15.9 \pm 28.2 \text{ pmol } \mu\text{mol m}^{-2}\text{s}^{-1}$  to  $12.9.4 \pm 31.717.5 \text{ pmol } \mu\text{mol m}^{-2}\text{s}^{-1}$  between May and October (Fig. 5a).  
 647 Periods between May and August of low (after cuts) and high (before cuts) LAI were compared as diel courses (Fig. 5). Over  
 648 the course of the day, both periods were characterized by a mean uptake of COS (Fig 5-6 c & d). Even though the uptake was  
 649 similar during nighttime, the daytime pattern differed considerably. The modelled contribution of the soil to the ecosystem  
 650 scale COS flux under high LAI conditions (Fig. 5-6 d) was minor, contributing between 1.3 % and 5.5/5.7 % of the  
 651 ecosystem flux during midday and morning/evening, respectively. In contrast, during low LAI conditions the soil  
 652 contribution to the ecosystem fluxes increased during daytime and contributed up to 8082.54% of the mean hourly COS  
 653 ecosystem flux (Fig 56. c). While the grassland acted as a stronger sink for COS during daytime at a high LAI, reaching peak  
 654 mean uptake values of up to  $-41.8 \text{ pmol m}^{-2}\text{s}^{-1} \pm 16.8 \text{ pmol m}^{-2}\text{s}^{-1}$  during midday, the mean daytime sink strength weakened  
 655 and we observed close to zero fluxes during midday in periods of low LAI. The magnitude of the soil flux ( $2 \pm 1 \text{ pmol m}^{-2}\text{s}^{-1}$ )  
 656 was not high enough to explain the difference variation of up to  $-23.726.0 \text{ pmol m}^{-2}\text{s}^{-1}$  between the measured COS  
 657 ecosystem flux and COS flux resulting from the FP+ model (Fig 5-6 c), suggesting a missing COS source. For phases of high  
 658 LAI we saw a good agreement between hourly averaged modelled and measured COS ecosystem fluxes (Fig 5-6 d). While  
 659 the grassland acted as a net sink for CO<sub>2</sub> during periods of high LAI (Fig. 5-6 b), a combination of a decline in GPP and an  
 660 increase in daytime RECO, as more incoming radiation was heating the soil surface, turned it into a net source during  
 661 midday in periods of low LAI (Fig. 5-6 a).  
 662



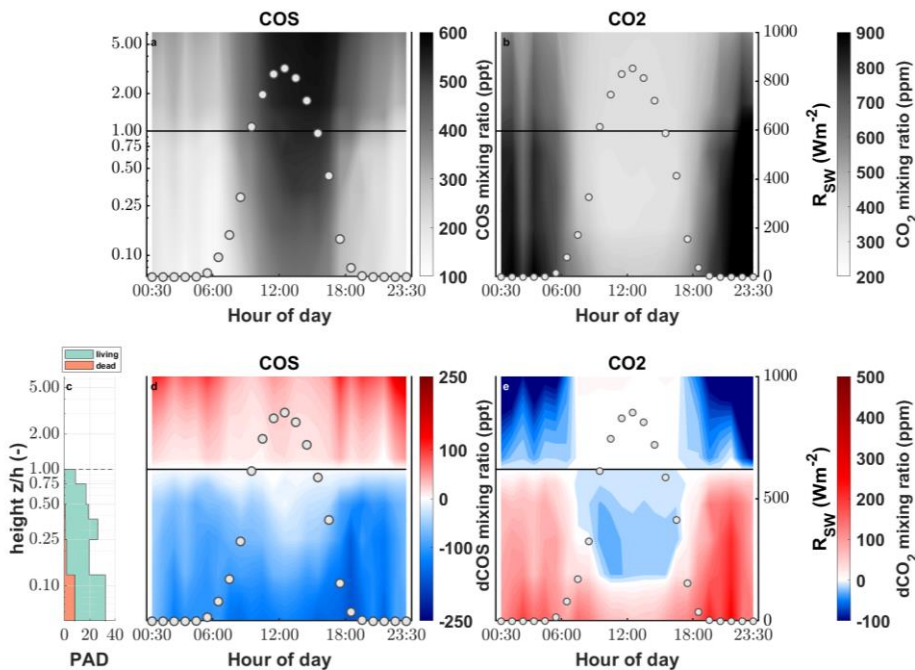
663  
 664 **Figure 56.** Mean diel variation of the measured and modelled CO<sub>2</sub> (a & b) and COS (c & d) fluxes for phases of low (LAI ≤3) (a & c)  
 665 and high (LAI ≥ 4) (b & d) from May to August. The carats depict the modelled gross primary productivity (blue), the modelled  
 666 ecosystem respiration (red) and the measured CO<sub>2</sub> ecosystem fluxes (black) in μmol m<sup>-2</sup>s<sup>-1</sup>. The circles depict the modelled COS soil flux  
 667 (yellow), the modelled COS ecosystem flux (turquoise) and the measured CO<sub>2</sub>-COS ecosystem fluxes (black) in pmol m<sup>-2</sup>s<sup>-1</sup>. The red area  
 668 depicts the difference between the measured ecosystem flux and the sum of the modelled fluxes. The grey areas depict the ±1 standard  
 669 deviation of the mean for all the measured fluxes. The white bars depict the diel mean total incoming shortwave radiation (W m<sup>-2</sup>s<sup>-1</sup>) while  
 670 the grey bars indicate the diel mean shortwave radiation reaching the soil surface.

671

### 672 3.4 COS mixing ratios above and within the canopy

673 While the canopy depleted the ambient  $\chi_{\text{CO}_2}$  during day as well as nighttime, we found that the  $\chi_{\text{CO}_2}$  reached values as low as  
 674 134 ppt (depletion of 102 ppt with respect to the mixing ratio at canopy height) during nighttime (see Fig. 6) at the bottom of  
 675 the canopy in contrast to the midday  $\chi_{\text{CO}_2}$ , which only went down to 389 ppt (depletion of 125 ppt with respect to the mixing  
 676 ratio at canopy height). We observed a decrease in  $\chi_{\text{CO}_2}$  (up to 26 ppm) within the most upper layers of the canopy compared  
 677 to  $\chi_{\text{CO}_2}$  at canopy height during daytime, while  $\chi_{\text{CO}_2}$  increased within the lowest layers compared to  $\chi_{\text{CO}_2}$  at the canopy height  
 678 due to soil respiration. The above-canopy  $\chi_{\text{CO}_2}$  increased considerably starting at the onset of the day and reached 587 ppt at  
 679 16:00. Over the course of the season the midday ambient  $\chi_{\text{CO}_2}$  decreased from 500 ± 28 ppt from mid-June to mid-July to  
 680 405 ± 29 ppt in October with the trend of increasing  $\chi_{\text{CO}_2}$  starting at the end of September (see Fig. S6).





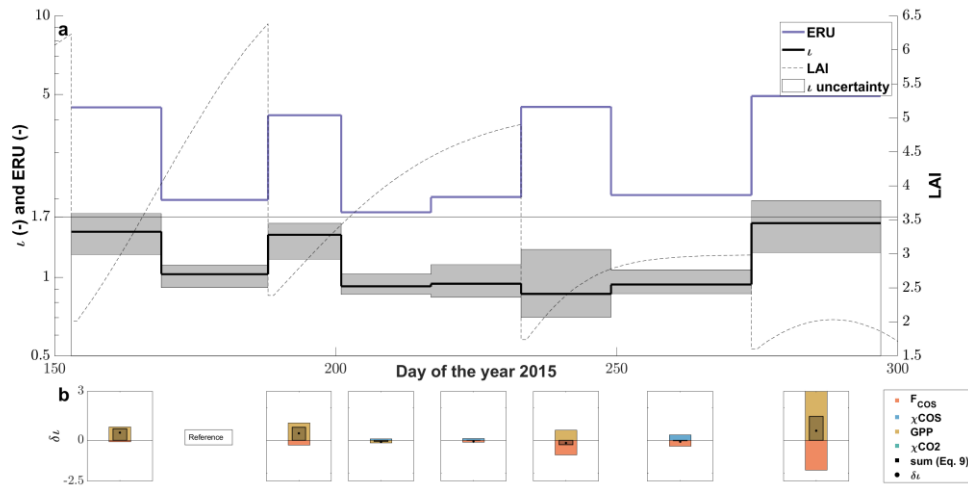
681  
 682 **Figure 6.** Vertical gradient of the (a) COS and (b) CO<sub>2</sub> mixing ratio (ppt and ppm, respectively) depicted by the background color between  
 683 the soil and the eddy covariance tower at 250 cm for one day. The left y axis shows the log of the measurement divided by the canopy  
 684 height (z/h). The white circles depict the incoming shortwave radiation ( $R_{sw}$ ) in ( $W \cdot m^{-2} \cdot s^{-1}$ ). Plant area density (PAD) split into living  
 685 (green) and dead (brown) plant material (c). Vertical gradient of the difference between the mixing ratio at canopy height and each  
 686 measurement height for (d) COS and (e) CO<sub>2</sub>.

687

### 688 3.5 Leaf and ecosystem relative uptake

689 The LRU at high-light conditions,  $\tau$ , which we calculated using the FP+ algorithm increased from relatively stable pre-cut  
 690 levels of 0.9-1.1 (-) ~~after-before~~ the 2<sup>nd</sup> and the 4<sup>th</sup>-1<sup>st</sup> cut to up to 1.5-6 (-) ~~after the 4<sup>th</sup> cut~~ (Fig. 7a). After the decrease in  $\tau$   
 691 between the 2<sup>nd</sup> and the 3<sup>rd</sup> cut,  $\tau$  increased steadily until the 4<sup>th</sup> cut, with the 3<sup>rd</sup> cut seemingly not having an effect. The  
 692 reason for the increase in  $\tau$  after the 2<sup>nd</sup> and 4<sup>th</sup> cut was a stronger decrease in GPP than the COS uptake, while both  
 693 decreased more evenly after the 3<sup>rd</sup> cut (Fig. 7b). We observed  $\tau$  in the period before the 4<sup>th</sup> cut to be influenced not only by a  
 694 decrease in COS uptake, but also by a decrease in COS mixing ratio (Fig 7b). The mean midday ERUs varied between  
 695 ~~4.92 ± 0.1 (-) before and 4.56 ± 0.3-4 (-) after the cuts-when excluding and 3.9 ± 1.3 (-) when including the first cut. The~~  
 696 ~~larger difference between the ERU and  $\tau$  after the cuts reflect that we observed similar respiration rates at low and high LAI~~  
 697 ~~(Fig 6a-b). The larger difference between the ERU and  $\tau$  after the cuts reflect the higher respiration rates of the ecosystem.~~  
 698 Under low light conditions, the LRU increased during pre- and post-cut phases in a similar manner with the last 15-day  
 699 period in October showing an earlier increase in the morning and evening (see Fig. S7).

700



701

702 **Figure 7.** (a) The seasonal cycle of  $\tau$  (black line) with the 95% confidence interval (gray area) resulting from the FP+ model and the  
 703 midday mean (11 a.m. – 2 p.m. at PAR > 800  $\mu\text{mol m}^{-2} \text{s}^{-1}$ ) ecosystem relative uptake (ERU) (blue line) using the  $\text{CO}_2$  ecosystem flux for  
 704 the calculation windows (~15 days adjusted to cuts). The dashed black line depicts the progression of the leaf area index (LAI) of the  
 705 grassland. (b) The contribution of the drivers ( $F_{\text{COS}}$ ,  $\chi_{\text{COS}}$ , GPP and  $\chi_{\text{CO}_2}$ ) to the changes in  $\tau$  between all calculation windows and the  
 706 reference period (DOY 169-188) resulting from the linear perturbation analysis compared to the observed change in  $\tau$  ( $\delta\tau$ ).

## 707 4 Discussion

### 708 4.1 COS mixing ratios

709 The continuous seasonal decrease in above-canopy  $\chi_{\text{COS}}$  from –500 ppt (in May) to –400 ppt (in October) was within the  
 710 range of published records observing mixing ratios to decrease from 465 (in summer) to 375 ppt (in winter) (Kuhn et al.,  
 711 1999). This pattern is typical for the northern hemisphere and the COS drawdown by terrestrial ecosystems (Montzka et al.,  
 712 2007). We found the lowest  $\chi_{\text{COS}}$  at the end of September, which coincides with the lowest ambient mixing ratios of COS,  
 713 measured in Ireland, the closest COS observation site Mace Head (MHD) of NOAA, on the 6<sup>th</sup> of October (Fig. S6).  
 714 The Gradient observations of the diurnal cycle revealed a continuous decrease of  $\chi_{\text{COS}}$  from the atmosphere (> 500ppt) down  
 715 to the soil reaching very low mixing ratios of 134 ppt during nighttime. extremely low COS canopy mixing ratios we  
 716 observed within the canopy, like this have also been reported by Rastogi et al. (2018), who measured a mean  $\chi_{\text{COS}}$  minimum  
 717 of 152 ppt at 1 m above the soil within an old growth forest. Compared to the consistent decrease of COS below the canopy  
 718 level during day and nighttime, the gradient for  $\text{CO}_2$  reverses during nighttime due to ongoing respiration processes while  
 719 plants are not photosynthetically active. Even though the COS mixing ratio at the layer closest to the soil were higher during  
 720 day than during nighttime, the absolute decrease in COS was lower during nighttime due to partial stomatal closure  
 721 (Kooijmans et al., 2017; Campbell et al., 2017). The absolute difference in concentrations during day and nighttime originate  
 722 from changes in the height of the planetary boundary layer (PBL). While the PBL is shallow during nighttime and the COS  
 723 mixing ratio decreases due to sink strength of the grassland, at the onset of the day, the PBL layer height increases fast and  
 724  $\text{CO}_2$  rich air is transported down to the ecosystem (Fig. S12) (Campbell et al., 2017). A similar steep increase until midday  
 725 has also been observed by Rastogi et al. (2018). Even though  $\text{CO}_2$  and COS share a similar pathway into plants, reflected by  
 726 their respective decrease in the mixing ratios within the canopy, we saw a difference at the lower levels of our gradient  
 727 analysis during daytime. We only observed an increase in  $\text{CO}_2$  mixing ratios, caused by the release of  $\text{CO}_2$  through  
 728 respiration processes in the soil, whereas COS mixing ratios further declined down to the soil surface. This supports our soil

Formatiert: Standard

Formatiert: Tiefgestellt

729 model, which predicted only minor COS fluxes under conditions of high LAI, when only a small portion of incident  
730 radiation reaches the soil surface.

#### 731 **4.1.2 Soil fluxes**

732 The nighttime soil chamber measurements compare well in terms of magnitude with the COS fluxes resulting from studies  
733 using dark chambers in agricultural and grassland sites (Whelan et al., 2018;Maseyk et al., 2014;Whelan and Rhew,  
734 2016;Liu et al., 2010) and indicate the soil to be a small sink for COS. The current understanding of COS soil exchange links  
735 the COS consumption to soil biota e.g. bacteria and fungi, possessing the ubiquitous enzyme CA (Kesselmeier et al.,  
736 1999;Meredith et al., 2019). ~~However, we also found 12 % of all nighttime fluxes to be emission.~~The origin of COS in soils  
737 on the other hand is still highly debated, but comparisons of untreated and sterilized soils suggest yet unknown abiotic  
738 processes (Meredith et al., 2019;Kitz et al., 2019).

739 ~~During daytime, the soil inside the chambers emitted COS at rates of up to 40.9 pmol m<sup>-2</sup>s<sup>-1</sup>. These~~The high COS emissions  
740 resulting from the soil chambers during daytime rates lie at the upper end of recently stated values of agricultural and  
741 grassland sites (Whelan et al., 2018;Kitz et al., 2017;Maseyk et al., 2014;Liu et al., 2010). Partly, this can be attributed to the  
742 type of chambers we used and their deployment. We allowed the full spectrum of incoming radiation to reach the soils  
743 surface, whereas most other studies used dark chambers. Therefore we were able to capture the influence of COS emission  
744 processes coupled to thermo- and photo production on our COS soil fluxes (Whelan and Rhew, 2015;Kitz et al.,  
745 2019;Meredith et al., 2018). This also led to lower peak soil emissions of COS at the end of the season, when the incoming  
746 radiation declined.

747 The low COS mixing ratios observed in the lowermost canopy layers just above the soil surface emphasize the importance of  
748 using air from within the canopy for soil chamber measurements and not COS richer air from above the canopy, which  
749 would increase the COS gradient and thus increase the uptake/decrease emission of COS to/from the soil.

750 Our modelled COS soil fluxes peak at about 12% of the maximum emissions retrieved from the soil chambers. This is owed  
751 to the difference in incident radiation reaching the soil surface between the fluxes resulting from chamber measurements and  
752 our model. For the chambers, the aboveground biomass was removed, whereas our modelled fluxes were adjusted for  
753 undisturbed canopy conditions. ~~In the gradient mixing ratio data, during pre-cut conditions, we also did not see an increase in~~  
754 COS mixing ratio within the canopy, which would have been a hint for a soil COS source.

755 Another factor contributing to the high COS soil emissions might be the yearly fertilization using slurry, as high nitrogen  
756 content in soils has been linked to a higher source strength of COS (Kaisermann et al., 2018). This agrees well with the study  
757 of Kitz et al. (2019), who found a correlation between increased soil nitrogen content and soil COS emission in a laboratory  
758 experiment with samples taken from the grassland at two different dates (i.e. June and September).

759

#### 760 **4.2.3 Ecosystem fluxes**

761 Our observations show that the agriculturally used grassland acted as a major sink for COS during the growing season. The  
762 fluxes fit well within or even exceeded the COS uptake rates of published grassland and agricultural sites during their  
763 growing phases (Billesbach et al., 2014;Whelan and Rhew, 2016;Geng and Mu, 2004). The late snow event that occurred in  
764 the peak growing season almost completely inhibited the exchange of CO<sub>2</sub> and COS, as the snow acted as a diffusion barrier  
765 for these compounds (Björkman et al., 2010).

766 The cuttings and the consecutive drying of the above ground plant material at the site had a major influence on the COS  
767 exchange. ~~During these events the grassland turned into a source for CO<sub>2</sub> and COS. COS emissions of a similar magnitude~~  
768 This hasve also been reported at agricultural fields in phases of senescence (Maseyk et al., 2014;Billesbach et al., 2014).

769 Although the soil was a strong source for COS, caused by the high R<sub>soil</sub> and T<sub>soil</sub> (Whelan and Rhew, 2015;Kitz et al.,

770 2019;Meredith et al., 2018), and the sink strength of the grassland was low due to the reduced aboveground biomass, soil  
771 fluxes did not explain the emission on ecosystem level (see Fig. 5a6a). As plants contain precursors involved in COS  
772 emission processes, e.g. methionine and cysteine (Meredith et al., 2018), the plant litter and dying plant parts remaining at  
773 the site after the cuts might be the missing source of COS. Laboratory tests of the soil of the grassland have shown that a  
774 mixing of dried litter and soil lead to a strong but short-lived emission peak of COS (Kitz et al., 2019). We did not observe  
775 strong COS emissions after the last cut, as the incoming solar radiation, which we hypothesize to amplify the degradation of  
776 sulfur containing compounds of plants, was reduced at the end of the season. Alternatively, the cutting of the grassland might  
777 induce stress mediated COS production in the remaining living plant parts (Bloem et al., 2012;Gimeno et al., 2017). The  
778 delay in the peak COS emissions at ecosystem scale after the cuts could indicate that some yet unknown biotic or abiotic  
779 processes take several days to release COS.

780 ~~We also observed another COS~~The short-lived timed-COS emission by yet unknown biotic or abiotic processes event shortly  
781 after the fertilization of the grassland towards the end of the growing season-- was likely triggered by ~~The~~ increase of  
782 available nitrogen (Kaisermann et al., 2018) and COS precursors introduced to the soil in the form of cattle slurry (Hörtnagl  
783 et al., 2018). ~~might have triggered the COS emission by biotic or abiotic processes.~~

784 Due to the independence of CA to catalyze COS without  $R_{PAR}$  (Stimler et al., 2011), the grassland remained a sink for COS  
785 during nighttime. Again, the soil sink was too small to explain the total COS exchange (Fig. 56), which indicates that the  
786 plant stomata were not fully closed (Kooijmans et al., 2017) and were responsible for the majority of the COS uptake. The  
787 minimum or residual stomatal conductances at the field site in Neustift have been reported to be between 10 and 65  $\text{mmol m}^{-2}$   
788  $\text{s}^{-1}$  depending on the species (Wohlfahrt, 2004).

789 The large variability in COS nighttime fluxes (Fig. 5c) is due to the combination of low wind speeds and stable stratification,  
790 which results in highly intermittent  $\text{CO}_2$  (Wohlfahrt et al., 2005) and COS fluxes compared to daytime. On half-hourly basis,  
791 even a nighttime net uptake of  $\text{CO}_2$  has been reported at the field site, which is typically compensated for by large  $\text{CO}_2$   
792 emissions in a subsequent averaging period (Wohlfahrt et al., 2005). We also observed this pattern for COS.

793 Although we observed phases of high VPD and low SWC (Fig. 1), they did not lead to a decrease in  $\text{CO}_2$  and COS  
794 ecosystem fluxes (Fig. S1-S2), which has already been observed for the grasslands  $\text{CO}_2$  and  $\text{H}_2\text{O}$  fluxes between 2001 and  
795 2009. The species located at the site were insensitive to progressive drought conditions (Brilli et al., 2011).

#### 796 **4.3 COS mixing ratios**

797 ~~The continuous decrease in above canopy  $\chi_{\text{COS}}$  from 500 ppt (in May) to 400 ppt (in October) is within the range of~~  
798 ~~published records observing mixing ratios to decrease from 465 (in summer) to 375 ppt (in winter) (Kuhn et al., 1999). This~~  
799 ~~pattern is typical for the northern hemisphere and the COS drawdown by terrestrial ecosystems (Montzka et al., 2007). We~~  
800 ~~found the lowest  $\chi_{\text{COS}}$  at the end of September, which coincides with the lowest ambient mixing ratios of COS, measured in~~  
801 ~~Ireland, the closest COS observation site Mace Head (MHD) of NOAA, on the 6<sup>th</sup> of October.~~

802 ~~Gradient observations of the diurnal cycle revealed a continuous decrease of  $\chi_{\text{COS}}$  from the atmosphere ( $> 500\text{ppt}$ ) down to~~  
803 ~~the soil reaching very low concentrations mixing ratios of 134 ppt during nighttime. Low values like this have also been~~  
804 ~~reported by Rastogi et al. (2018), who measured a mean  $\chi_{\text{COS}}$  minimum of 152 ppt at 1 m above the soil within an old growth~~  
805 ~~forest. The difference in concentrations during day and nighttime originates from changes in the height of the planetary~~  
806 ~~boundary layer (PBL). While the PBL is shallow during nighttime and the COS mixing ratio decreases due to sink strength~~  
807 ~~of the grassland, at the onset of the day, the PBL layer height increases fast and COS rich air is transported down to the~~  
808 ~~ecosystem. Even though  $\text{CO}_2$  and COS share a similar pathway into plants, reflected by their respective decrease in the~~  
809 ~~mixing ratios within the canopy, we saw a difference at the lower levels of our gradient analysis during daytime. We only~~  
810 ~~observed an increase in  $\text{CO}_2$  mixing ratios, caused by the release of  $\text{CO}_2$  through respiration processes in the soil, whereas~~

811 ~~COS mixing ratios further declined down to the soil surface. This supports our soil model, which predicted only minor COS~~  
812 ~~fluxes under conditions of high LAI, when only a small portion of incident radiation was hitting the soil surface.~~

#### 813 4.4 LRU

814 The parameter  $\tau$  ~~varied between 0.9 (0.8–1.0) (-) and 1.5 (1.2–1.8) (-) during the campaign, where cuts of the grassland tended~~  
815 ~~to result in higher values and of places~~ this study is placed at the lower end of a recent compilation of all published leaf-level  
816 LRUs, that put 95% of all data between 0.7 (-) and 6.2 (-) with a median of 1.7 (-) (Whelan et al., 2018) and also lower than  
817 the LRU of 2.53 (-) estimated for grasslands by Seibt et al. (2010). ~~Even the higher  $\tau$  after the cuts was low compared to~~  
818 ~~these studies.~~ The seasonal trend of ~~the LRUs  $\tau$~~  was strongly influenced by the cutting of the grass and can be attributed  
819 mainly to changes in the ratio of COS uptake to GPP. However, we also observed a strong decline in the ambient mixing  
820 ratio of COS, which also had an equally strong influence on the change in  $\tau$  as the COS flux for the 15 day window before  
821 the last cut (Fig 7 b).

822 Even though the changes in  $\tau$  can be explained, it is important to keep in mind that the grassland was a source for COS on  
823 ecosystem level after the cuts. For the calculation of LRUs we had to remove ~~those the canopy flux data containing COS~~  
824 ~~and/or CO<sub>2</sub> emissions observations from the data~~ since they would yield negative values for ERU and LRU (see Eq.8). This  
825 indicates that the unknown source strength after cuts likely decreases the post-cut  $\tau$ 's.

#### 826 5 Conclusion

827 Due to the management interventions at the grassland site, the leaf area development was decoupled from seasonal changes  
828 in environmental forcing. This allowed us to measure concurrent CO<sub>2</sub> and COS fluxes at soil and ecosystem level for  
829 multiple growing periods within one season. The LAI on seasonal scale as well as incoming solar radiation on hourly to  
830 seasonal scales determined whether soils were a source or a sink for COS. The incoming shortwave radiation reaching the  
831 soil surface had a decisive influence on the COS soil surface flux and thus supports our hypothesis H4. The covariance  
832 between the daytime CO<sub>2</sub> and COS fluxes on daily to seasonal level was high and the fluxes only diverged after the cuts,  
833 leading to higher LRUs. Beside the perturbations of the ecosystem, the sink strength of the grassland was high for COS and  
834 declined over the course of the season (H1). The COS emissions at ecosystem scale shortly after the cuts, which could not be  
835 explained by the soil source, raise questions about other unknown mechanisms of COS production within ecosystems (H2).  
836 With the exception of short periods after the cuts, the LRUs under high light conditions were relatively constant during the  
837 season, indicating a good correlation between the COS flux and GPP under stable conditions (H3).

#### 838 6. Data availability

839 Data and materials availability: <https://doi.org/10.5281/zenodo.3886554> ~~Will be uploaded to <https://zenodo.org/>~~

840

#### 841 7. Author contributions

842 Felix M. Spielmann: Data curation, Formal analysis, Investigation, Methodology, Software, Visualization, Writing – original  
843 draft

844 Albin Hammerle: Data curation, Investigation, Software, Writing – original draft

845 Florian Kitz: Data curation, Formal analysis, Investigation, Methodology, Software, Writing – original draft

846 Katharina Gerdel: Investigation, Software, Writing – original draft

Formatiert: Schriftart: Symbol

Formatiert: Schriftart: Symbol

847 Georg Wohlfahrt: Conceptualization, Funding acquisition, Investigation, Methodology, Project administration, Software,  
848 Supervision, Writing – original draft

## 849 8. Competing interests

850 The authors declare no competing financial interests.

## 851 9. Acknowledgements

852 This study was financially supported by the Austrian National Science Fund (FWF; contracts P26931, P27176, and I03859),  
853 the Tyrolean Science Fund (contract UNI-0404/1801), and the University of Innsbruck (Infrastructure funding by Research  
854 Area Alpine Space-Man and Environment to G. W). Financial support to F. M. S. was provided through a PhD scholarship  
855 by the University of Innsbruck. We thank family Hofer (Neustift, Austria) for kindly granting us access to the study site.  
856 COS flask data were provided by the Global Monitoring Division of the National Oceanic and Atmospheric  
857 Administration's Earth System Research Laboratory (NOAA ESRL/GMD). The authors declare no competing financial  
858 interests.

## 859 10. References

- 860 Asaf, D., Rotenberg, E., Tatarinov, F., Dicken, U., Montzka, S. A., and Yakir, D.: Ecosystem photosynthesis inferred from  
861 measurements of carbonyl sulphide flux, *Nature Geoscience*, 6, 186-190, 10.1038/ngeo1730, 2013.
- 862 Aubinet, M., Grelle, A., Ibrom, A., Rannik, Ü., Moncrieff, J., Foken, T., Kowalski, A. S., Martin, P. H., Berbigier, P.,  
863 Bernhofer, C., Clement, R., Elbers, J., Granier, A., Grünwald, T., Morgenstern, K., Pilegaard, K., Rebmann, C.,  
864 Snijders, W., Valentini, R., and Vesala, T.: Estimates of the Annual Net Carbon and Water Exchange of Forests:  
865 The EUROFLUX Methodology, in: *Advances in Ecological Research Volume 30*, edited by: Fitter, A. H., and  
866 Raffaelli, D. G., *Advances in Ecological Research*, Academic Press, 113-175, 1999.
- 867 Baldocchi, D.: Measuring fluxes of trace gases and energy between ecosystems and the atmosphere - the state and future of  
868 the eddy covariance method, *Glob Chang Biol*, 20, 3600-3609, doi.org/10.1111/gcb.12649, 2014.
- 869 Billesbach, D. P., Berry, J. A., Seibt, U., Maseyk, K., Torn, M. S., Fischer, M. L., Abu-Naser, M., and Campbell, J. E.:  
870 Growing season eddy covariance measurements of carbonyl sulfide and CO<sub>2</sub> fluxes: COS and CO<sub>2</sub> relationships in  
871 Southern Great Plains winter wheat, *Agricultural and Forest Meteorology*, 184, 48-55,  
872 10.1016/j.agrformet.2013.06.007, 2014.
- 873 Björkman, M. P., Morgner, E., Cooper, E. J., Elberling, B., Klemetsson, L., and Björk, R. G.: Winter carbon dioxide  
874 effluxes from Arctic ecosystems: An overview and comparison of methodologies, *Global Biogeochemical Cycles*,  
875 24, 10.1029/2009gb003667, 2010.
- 876 Bloem, E., Haneklaus, S., Kesselmeier, J., and Schnug, E.: Sulfur Fertilization and Fungal Infections Affect the Exchange of  
877 H<sub>2</sub>S and COS from Agricultural Crops, *Journal of Agricultural and Food Chemistry*, 60, 7588-7596,  
878 10.1021/jf301912h, 2012.
- 879 Brilli, F., Hörtnagl, L., Hammerle, A., Haslwanter, A., Hansel, A., Loreto, F., and Wohlfahrt, G.: Leaf and ecosystem  
880 response to soil water availability in mountain grasslands, *Agricultural and Forest Meteorology*, 151, 1731-1740,  
881 doi.org/10.1016/j.agrformet.2011.07.007, 2011.
- 882 Brühl, C., Lelieveld, J., Crutzen, P. J., and Tost, H.: The role of carbonyl sulphide as a source of stratospheric sulphate  
883 aerosol and its impact on climate, *Atmos. Chem. Phys.*, 12, 1239-1253, 10.5194/acp-12-1239-2012, 2012.
- 884 Campbell, J. E., Whelan, M. E., Berry, J. A., Hilton, T. W., Zumkehr, A., Stinecipher, J., Lu, Y., Kornfeld, A., Seibt, U.,  
885 Dawson, T. E., Montzka, S. A., Baker, I. T., Kulkarni, S., Wang, Y., Herndon, S. C., Zahniser, M. S., Commane,  
886 R., and Loik, M. E.: Plant Uptake of Atmospheric Carbonyl Sulfide in Coast Redwood Forests, *Journal of*  
887 *Geophysical Research-Biogeosciences*, 122, 3391-3404, 10.1002/2016jg003703, 2017.
- 888 Ensign, S. A.: Reactivity of Carbon Monoxide Dehydrogenase from *Rhodospirillum rubrum* with Carbon Dioxide, Carbonyl  
889 Sulfide, and Carbon Disulfide, *Biochemistry*, 34, 5372-5381, 10.1021/bi00016a008, 1995.
- 890 Geng, C., and Mu, Y.: Carbonyl sulfide and dimethyl sulfide exchange between lawn and the atmosphere, *Journal of*  
891 *Geophysical Research: Atmospheres*, 109, 10.1029/2003jd004492, 2004.
- 892 Gerdel, K., Spielmann, F. M., Hammerle, A., and Wohlfahrt, G.: Eddy covariance carbonyl sulfide flux measurements with a  
893 quantum cascade laser absorption spectrometer, *Atmospheric Measurement Techniques*, 10, 3525-3537,  
894 10.5194/amt-10-3525-2017, 2017.
- 895 Gimeno, T. E., Ogee, J., Royles, J., Gibon, Y., West, J. B., Burlett, R., Jones, S. P., Sauze, J., Wohl, S., Benard, C., Genty,  
896 B., and Wingate, L.: Bryophyte gas-exchange dynamics along varying hydration status reveal a significant carbonyl

897 sulphide (COS) sink in the dark and COS source in the light, *New Phytologist*, 215, 965-976, 10.1111/nph.14584,  
898 2017.

899 Hortnagl, L., Clement, R., Graus, M., Hammerle, A., Hansel, A., and Wohlfahrt, G.: Dealing with disjunct concentration  
900 measurements in eddy covariance applications: A comparison of available approaches, *Atmospheric Environment*,  
901 44, 2024-2032, 10.1016/j.atmosenv.2010.02.042, 2010.

902 Hörtnagl, L., Barthel, M., Buchmann, N., Eugster, W., Butterbach-Bahl, K., Díaz-Pinés, E., Zeeman, M., Klumpp, K., Kiese,  
903 R., Bahn, M., Hammerle, A., Lu, H., Ladreiter-Knauss, T., Burri, S., and Merbold, L.: Greenhouse gas fluxes over  
904 managed grasslands in Central Europe, *Global Change Biology*, 24, 1843-1872, 10.1111/gcb.14079, 2018.

905 Kaisermann, A., Jones, S., Wohl, S., Ogée, J., and Wingate, L.: Nitrogen Fertilization Reduces the Capacity of Soils to Take  
906 up Atmospheric Carbonyl Sulphide, *Soil Syst.*, 2, 10.3390/soilsystems2040062, 2018.

907 Kesselmeier, J., Teusch, N., and Kuhn, U.: Controlling variables for the uptake of atmospheric carbonyl sulfide by soil, *J.*  
908 *Geophys. Res.-Atmos.*, 104, 11577-11584, 10.1029/1999jd900090, 1999.

909 Kitz, F., Gerdel, K., Hammerle, A., Laterza, T., Spielmann, F. M., and Wohlfahrt, G.: In situ soil COS exchange of a  
910 temperate mountain grassland under simulated drought, *Oecologia*, 1-10, 10.1007/s00442-016-3805-0, 2017.

911 Kitz, F., Gómez-Brandón, M., Eder, B., Etemadi, M., Spielmann, F. M., Hammerle, A., Insam, H., and Wohlfahrt, G.: Soil  
912 carbonyl sulfide exchange in relation to microbial community composition: Insights from a managed grassland soil  
913 amendment experiment, *Soil Biology and Biochemistry*, 135, 28-37, 10.1016/j.soilbio.2019.04.005, 2019.

914 Kooijmans, L. M. J., Uitslag, N. A. M., Zahniser, M. S., Nelson, D. D., Montzka, S. A., and Chen, H. L.: Continuous and  
915 high-precision atmospheric concentration measurements of COS, CO<sub>2</sub>, CO and H<sub>2</sub>O using a quantum cascade laser  
916 spectrometer (QCLS), *Atmospheric Measurement Techniques*, 9, 5293-5314, 10.5194/amt-9-5293-2016, 2016.

917 Kooijmans, L. M. J., Maseyk, K., Seibt, U., Sun, W., Vesala, T., Mammarella, I., Kolari, P., Aalto, J., Franchin, A., Vecchi,  
918 R., Valli, G., and Chen, H.: Canopy uptake dominates nighttime carbonyl sulfide fluxes in a boreal forest, *Atmos.*  
919 *Chem. Phys.*, 17, 11453-11465, 10.5194/acp-17-11453-2017, 2017.

920 Kooijmans, L. M. J., Sun, W., Aalto, J., Erkkilä, K. M., Maseyk, K., Seibt, U., Vesala, T., Mammarella, I., and Chen, H.:  
921 Influences of light and humidity on carbonyl sulfide-based estimates of photosynthesis, *Proc Natl Acad Sci U S A*,  
922 10.1073/pnas.1807600116, 2019.

923 Krysztofiak, G., Té, Y. V., Catoire, V., Berthet, G., Toon, G. C., Jégou, F., Jeseck, P., and Robert, C.: Carbonyl Sulphide  
924 (OCS) Variability with Latitude in the Atmosphere, *Atmosphere-Ocean*, 53, 89-101,  
925 10.1080/07055900.2013.876609, 2015.

926 Kuhn, U., Ammann, C., Wolf, A., Meixner, F. X., Andreae, M. O., and Kesselmeier, J.: Carbonyl sulfide exchange on an  
927 ecosystem scale: soil represents a dominant sink for atmospheric COS, *Atmospheric Environment*, 33, 995-1008,  
928 Doi 10.1016/S1352-2310(98)00211-8, 1999.

929 Langford, B., Acton, W., Ammann, C., Valach, A., and Nemitz, E.: Eddy-covariance data with low signal-to-noise ratio:  
930 time-lag determination, uncertainties and limit of detection, *Atmospheric Measurement Techniques*, 8, 4197-4213,  
931 10.5194/amt-8-4197-2015, 2015.

932 Lasslop, G., Reichstein, M., Papale, D., Richardson, A. D., Arneth, A., Barr, A., Stoy, P., and Wohlfahrt, G.: Separation of  
933 net ecosystem exchange into assimilation and respiration using a light response curve approach: critical issues and  
934 global evaluation, *Global Change Biology*, 16, 187-208, 10.1111/j.1365-2486.2009.02041.x, 2010.

935 Le Quere, C., Andrew, R. M., Friedlingstein, P., Sitch, S., Pongratz, J., Manning, A. C., Korsbakken, J. I., Peters, G. P.,  
936 Canadell, J. G., Jackson, R. B., Boden, T. A., Tans, P. P., Andrews, O. D., Arora, V. K., Bakker, D. C. E., Barbero,  
937 L., Becker, M., Betts, R. A., Bopp, L., Chevallier, F., Chini, L. P., Ciais, P., Cosca, C. E., Cross, J., Currie, K.,  
938 Gasser, T., Harris, I., Hauck, J., Haverd, V., Houghton, R. A., Hunt, C. W., Hurtt, G., Ilyina, T., Jain, A. K., Kato,  
939 E., Kautz, M., Keeling, R. F., Goldewijk, K. K., Kortzinger, A., Landschutzer, P., Lefevre, N., Lenton, A., Lienert,  
940 S., Lima, I., Lombardozzi, D., Metzl, N., Miller, F., Monteiro, P. M. S., Munro, D. R., Nabel, J., Nakaoka, S.,  
941 Nojiri, Y., Padin, X. A., Peregón, A., Pfeil, B., Pierrot, D., Poulter, B., Rehder, G., Reimer, J., Rodenbeck, C.,  
942 Schwinger, J., Seferian, R., Skjelvan, I., Stocker, B. D., Tian, H. Q., Tilbrook, B., Tubiello, F. N., van der Laan-  
943 Luijkx, I. T., van der Werf, G. R., van Heuven, S., Viovy, N., Vuichard, N., Walker, A. P., Watson, A. J., Wiltshire,  
944 A. J., Zaehle, S., and Zhu, D.: Global Carbon Budget 2017, *Earth System Science Data*, 10, 405-448, 10.5194/essd-  
945 10-405-2018, 2018.

946 Liaw, A., and Wiener, M.: Classification and Regression by RandomForest, *R News*, 2/3, 18-22, 2002.

947 Liu, J., Geng, C., Mu, Y., Zhang, Y., Xu, Z., and Wu, H.: Exchange of carbonyl sulfide (COS) between the atmosphere and  
948 various soils in China, *Biogeosciences*, 7, 753-762, 10.5194/bg-7-753-2010, 2010.

949 Lorimer, G. H., and Pierce, J.: Carbonyl sulfide: an alternate substrate for but not an activator of ribulose-1,5-bisphosphate  
950 carboxylase, *The Journal of biological chemistry*, 264, 2764-2772, 1989.

951 Maseyk, K., Berry, J. A., Billesbach, D., Campbell, J. E., Torn, M. S., Zahniser, M., and Seibt, U.: Sources and sinks of  
952 carbonyl sulfide in an agricultural field in the Southern Great Plains, *Proceedings of the National Academy of*  
953 *Sciences of the United States of America*, 111, 9064-9069, 10.1073/pnas.1319132111, 2014.

954 Meredith, L. K., Boye, K., Youngerman, C., Whelan, M., Ogée, J., Sauze, J., and Wingate, L.: Coupled Biological and  
955 Abiotic Mechanisms Driving Carbonyl Sulfide Production in Soils, *Soil Syst.*, 2, 27, 10.3390/soilsystems2030037,  
956 2018.

957 Meredith, L. K., Ogée, J., Boye, K., Singer, E., Wingate, L., von Sperber, C., Sengupta, A., Whelan, M., Pang, E., Keiluweit,  
958 M., Brüggemann, N., Berry, J. A., and Welander, P. V.: Soil exchange rates of COS and CO<sub>18</sub>O differ with the  
959 diversity of microbial communities and their carbonic anhydrase enzymes, *The ISME Journal*, 13, 290-300,  
960 10.1038/s41396-018-0270-2, 2019.



961 Montzka, S. A., Calvert, P., Hall, B. D., Elkins, J. W., Conway, T. J., Tans, P. P., and Sweeney, C.: On the global  
962 distribution, seasonality, and budget of atmospheric carbonyl sulfide (COS) and some similarities to CO<sub>2</sub>, *J.*  
963 *Geophys. Res.-Atmos.*, 112, 10.1029/2006jd007665, 2007.

964 Notni, J., Schenk, S., Protoschill-Krebs, G., Kesselmeier, J., and Anders, E.: The missing link in COS metabolism: a model  
965 study on the reactivation of carbonic anhydrase from its hydrosulfide analogue, *Chembiochem : a European journal*  
966 *of chemical biology*, 8, 530-536, 10.1002/cbic.200600436, 2007.

967 Ogawa, T., Noguchi, K., Saito, M., Nagahata, Y., Kato, H., Ohtaki, A., Nakayama, H., Dohmae, N., Matsushita, Y., Odaka,  
968 M., Yohda, M., Nyunoya, H., and Katayama, Y.: Carbonyl Sulfide Hydrolase from *Thiobacillus thioparus* Strain  
969 TH115 Is One of the  $\beta$ -Carbonic Anhydrase Family Enzymes, *Journal of the American Chemical Society*, 135,  
970 3818-3825, 10.1021/ja307735e, 2013.

971 Protoschill-Krebs, G., and Kesselmeier, J.: ENZYMATIC PATHWAYS FOR THE CONSUMPTION OF CARBONYL  
972 SULFIDE (COS) BY HIGHER-PLANTS, *Botanica Acta*, 105, 206-212, 1992.

973 Rastogi, B., Berkelhammer, M., Wharton, S., Whelan, M. E., Itter, M. S., Leen, J. B., Gupta, M. X., Noone, D., and Still, C.  
974 J.: Large Uptake of Atmospheric OCS Observed at a Moist Old Growth Forest: Controls and Implications for  
975 Carbon Cycle Applications, *Journal of Geophysical Research-Biogeosciences*, 123, 3424-3438,  
976 10.1029/2018jg004430, 2018.

977 Sandoval-Soto, L., Stanimirov, M., von Hobe, M., Schmitt, V., Valdes, J., Wild, A., and Kesselmeier, J.: Global uptake of  
978 carbonyl sulfide (COS) by terrestrial vegetation: Estimates corrected by deposition velocities normalized to the  
979 uptake of carbon dioxide (CO<sub>2</sub>), *Biogeosciences*, 2, 125-132, 10.5194/bg-2-125-2005, 2005.

980 Seefeldt, L. C., Rasche, M. E., and Ensign, S. A.: Carbonyl sulfide and carbon dioxide as new substrates, and carbon  
981 disulfide as a new inhibitor, of nitrogenase, *Biochemistry*, 34, 5382-5389, 10.1021/bi00016a009, 1995.

982 Seibt, U., Kesselmeier, J., Sandoval-Soto, L., Kuhn, U., and Berry, J.: A kinetic analysis of leaf uptake of COS and its  
983 relation to transpiration, photosynthesis and carbon isotope fractionation, *Biogeosciences*, 7, 333-341, 2010.

984 Smeulders, M. J., Pol, A., Venselaar, H., Barends, T. R. M., Hermans, J., Jetten, M. S. M., and Op den Camp, H. J. M.:  
985 Bacterial CS<sub>2</sub> Hydrolases from *Acidithiobacillus thiooxidans* Strains Are Homologous to the  
986 Archaeal Catenane CS<sub>2</sub> Hydrolase, *Journal of Bacteriology*, 195, 4046, 10.1128/JB.00627-  
987 13, 2013.

989 Spielmann, F. M., Wohlfahrt, G., Hammerle, A., Kitz, F., Migliavacca, M., Alberti, G., Ibrom, A., El-Madany, T. S., Gerdel,  
990 K., Moreno, G., Kolle, O., Karl, T., Peressotti, A., and Delle Vedove, G.: Gross Primary Productivity of Four  
991 European Ecosystems Constrained by Joint CO<sub>2</sub> and COS Flux Measurements, *Geophys. Res. Lett.*, 0,  
992 10.1029/2019gl082006, 2019.

993 Stimler, K., Berry, J. A., Montzka, S. A., and Yakir, D.: Association between Carbonyl Sulfide Uptake and (18)Delta during  
994 Gas Exchange in C-3 and C-4 Leaves, *Plant Physiology*, 157, 509-517, 10.1104/pp.111.176578, 2011.

995 Stoy, P. C., Katul, G. G., Siqueira, M. B. S., Juang, J. Y., Novick, K. A., McCarthy, H. R., Oishi, A. C., Uebelherr, J. M.,  
996 Kim, H. S., and Oren, R.: Separating the effects of climate and vegetation on evapotranspiration along a  
997 successional chronosequence in the southeastern US, *Global Change Biology*, 12, 2115-2135, 10.1111/j.1365-  
998 2486.2006.01244.x, 2006.

999 Tucker, C. J.: Red and photographic infrared linear combinations for monitoring vegetation, *Remote Sensing of*  
1000 *Environment*, 8, 127-150, [https://doi.org/10.1016/0034-4257\(79\)90013-0](https://doi.org/10.1016/0034-4257(79)90013-0), 1979.

1001 Whelan, M. E., and Rhew, R. C.: Carbonyl sulfide produced by abiotic thermal and photodegradation of soil organic matter  
1002 from wheat field substrate, *Journal of Geophysical Research-Biogeosciences*, 120, 54-62, 10.1002/2014jg002661,  
1003 2015.

1004 Whelan, M. E., and Rhew, R. C.: Reduced sulfur trace gas exchange between a seasonally dry grassland and the atmosphere,  
1005 *Biogeochemistry*, 128, 267-280, 10.1007/s10533-016-0207-7, 2016.

1006 Whelan, M. E., Lennartz, S. T., Gimeno, T. E., Wehr, R., Wohlfahrt, G., Wang, Y., Kooijmans, L. M. J., Hilton, T. W.,  
1007 Belviso, S., Peylin, P., Commane, R., Sun, W., Chen, H., Kuai, L., Mammarella, I., Maseyk, K., Berkelhammer, M.,  
1008 Li, K. F., Yakir, D., Zumkehr, A., Katayama, Y., Ogée, J., Spielmann, F. M., Kitz, F., Rastogi, B., Kesselmeier, J.,  
1009 Marshall, J., Erkkilä, K. M., Wingate, L., Meredith, L. K., He, W., Bunk, R., Launois, T., Vesala, T., Schmidt, J. A.,  
1010 Fichot, C. G., Seibt, U., Saleska, S., Saltzman, E. S., Montzka, S. A., Berry, J. A., and Campbell, J. E.: Reviews and  
1011 syntheses: Carbonyl sulfide as a multi-scale tracer for carbon and water cycles, *Biogeosciences*, 15, 3625-3657,  
1012 10.5194/bg-15-3625-2018, 2018.

1013 Wohlfahrt, G., Bahn, M., Tappeiner, U., and Cernusca, A.: A multi-component, multi-species model of vegetation-  
1014 atmosphere CO<sub>2</sub> and energy exchange for mountain grasslands, *Agricultural and Forest Meteorology*, 106, 261-  
1015 287, 10.1016/s0168-1923(00)00224-0, 2001.

1016 Wohlfahrt, G.: Modelling fluxes and concentrations of CO<sub>2</sub>, H<sub>2</sub>O and sensible heat within and above a mountain meadow  
1017 canopy: A comparison of three Lagrangian models and three parameterisation options for the Lagrangian time  
1018 scale, *Boundary-Layer Meteorology*, 113, 43-80, 10.1023/B:BOUN.0000037326.40490.1f, 2004.

1019 Wohlfahrt, G., Anfang, C., Bahn, M., Haslwanter, A., Newsely, C., Schmitt, M., Drosler, M., Pfadenhauer, J., and  
1020 Cernusca, A.: Quantifying nighttime ecosystem respiration of a meadow using eddy covariance, chambers and  
1021 modelling, *Agricultural and Forest Meteorology*, 128, 141-162, 10.1016/j.agrformet.2004.11.003, 2005.

1022 Wohlfahrt, G., Hammerle, A., Haslwanter, A., Bahn, M., Tappeiner, U., and Cernusca, A.: Seasonal and inter-annual  
1023 variability of the net ecosystem CO<sub>2</sub> exchange of a temperate mountain grassland: Effects of weather and  
1024 management, *Journal of Geophysical Research: Atmospheres*, 113, 10.1029/2007jd009286, 2008.



1025 Wohlfahrt, G., Brilli, F., Hoertnagl, L., Xu, X., Bingemer, H., Hansel, A., and Loreto, F.: Carbonyl sulfide (COS) as a tracer  
1026 for canopy photosynthesis, transpiration and stomatal conductance: potential and limitations, *Plant Cell and*  
1027 *Environment*, 35, 657-667, 10.1111/j.1365-3040.2011.02451.x, 2012.  
1028 Yang, F., Qubaja, R., Tatarinov, F., Rotenberg, E., and Yakir, D.: Assessing canopy performance using carbonyl sulfide  
1029 measurements, *Global Change Biology*, 24, 3486-3498, doi:10.1111/gcb.14145, 2018.  
1030